THE GEOLOGICAL SOCIETY OF AMERICA®

A waning Saxothuringian Ocean evidenced in the Famennian tephra-bearing siliceous succession of the Bardo Unit (Central Sudetes, SW Poland)

Grzegorz Racki[1,†], Stanisław Mazur[2], Katarzyna Narkiewicz[3], Agnieszka Pisarzowska[1], Waldemar Bardziński[1], Katarzyna Kołtonik[4], Dawid Szymanowski[5], Paweł Filipiak[1], and Barbara Kremer[6]

[1]*Institute of Earth Sciences, University of Silesia in Katowice, Będzińska 60, 41-200 Sosnowiec, Poland*
[2]*Institute of Geological Sciences, Polish Academy of Sciences, Kraków Research Centre, Senacka 1, 31-002 Kraków, Poland*
[3]*Polish Geological Institute-National Research Institute, Rakowiecka t 4, 00-975 Warszawa, Poland*
[4]*Institute of Nuclear Physics, Polish Academy of Sciences, Radzikowskiego 152, 31-342 Kraków, Poland*
[5]*Department of Geosciences, Princeton University, Guyot Hall, Princeton, New Jersey 08544, USA*
[6]*Institute of Paleobiology, Polish Academy of Sciences, Twarda 51/55, 00-818 Warszawa, Poland*

ABSTRACT

A tephra-rich cherty-clayey Famennian succession within the major Brzeźnica olistostrome in the Bardo Mountains, Central Sudetes, SW Poland, preserves a record of the lost ocean later incorporated into the Variscan orogenic belt. Fluctuating but mostly oligotrophic regimes and low primary production levels were influenced by weak upwelling below the perennial oxygen minimum zone, which controlled the interplay between biosiliceous and siliciclastic deposition in the oceanic basin, with episodic oxygen deficiency. The Hangenberg Black Shale has been identified in this oceanic setting based on its characteristics described worldwide (including mercury enrichments). A tectonic uplift of the sediment source area near the Devonian-Carboniferous boundary, recorded in the distinguishing provenance signal of old continental crust, was paired with a global transgression, anoxia, and volcanic episode in an interglacial interval. Assuming paleogeographic affinity with the Bavarian facies of the Saxothuringian terrane, we interpret the allochthonous sediments as part of an accretionary prism that was gravitationally redeposited into the late orogenic basin in front of advancing Variscan nappes. The oceanic basin parental to the Bardo pelagic succession is therefore thought to represent a tract of the waning Saxothuringian Ocean in the Peri-Gondwanan paleogeographic domain that was eventually subducted beneath the Brunovistulian margin of Laurussia. The sediments of the Bardo Ocean basin also include a distal record of Famennian explosive volcanic activity that was likely related to a continental magmatic arc whose remnants are preserved as the Vrbno Group of the East Sudetes.

INTRODUCTION

Biosiliceous facies in middle Paleozoic deep-water, partly oceanic basins are widespread (Hein and Parrish, 1987), but the depositional record of Late Devonian radiolarian oozes remains poorly known. Unlike the common Early Carboniferous Kulm facies (Tournaisian hypersiliceous period of Racki and Cordey, 2000, their fig. 3; see Gursky, 1996; Randon and Caridroit, 2008), Late Devonian pelagic cherty strata of Variscan Europe are overwhelmingly lost to a pervasive tectonic or metamorphic overprint (Kiessling and Tragelehn, 1994).

We report data from a hemipelagic siliceous succession with pyroclastic horizons found in the Bardo Mountains (Góry Bardzkie), one of the main structural units of the Central Sudetes, SW Poland (Figs. 1A and 1B). This fault-bounded complex rock suite is defined as the Bardo Sedimentary Unit (Mazur et al., 2006) or Bardo Fold Structure (Żelaźniewicz et al., 2011), an element of the Saxothuringian Zone on the northern flank of the European Variscides (Franke et al., 1993, 2017) consisting of poorly outcropped, dismembered sedimentary series ranging in age from the Upper Ordovician to lowermost Upper Carboniferous (Haydukiewicz, 1979, 1990; Oberc, 1980; Cymerman et al., 2015; Fig. 1C). According to Wajsprych (1978, 1986, 2008), autochthonous and allochthonous litho-tectonic domains are clearly distinguished in this oceanic succession. Early Carboniferous (late Viséan) wildflysch deposits include flysch-dominated sediments, biostratigraphically dated by graptolites and conodonts as Silurian and Devonian in age (see summary in Haydukiewicz, 1990, 1998; Cymerman et al., 2015).

New litho- and biostratigraphic data from the Bavarian-type section of the Bardo Basin sediments are integrated with zircon geochronology on intercalated tephra. The characteristics of the Famennian explosive volcanism potentially link this activity to continental arc magmatism in the East Sudetes (Janoušek et al., 2014). The results are important in the context of controversial paleogeography between Gondwana and Laurussia (Franke et al., 1993, 1995, 2017; Romer and Hahne, 2010; Mazur et al., 2015; Golonka, 2020), and the global Devonian-Carboniferous Hangenberg biotic crisis (Walliser, 1996; Aretz, 2020) uniquely identifiable in the easternmost part of the Saxothuringian Zone.

GEOLOGICAL SETTING

The sedimentary succession of the Bardo Basin comprises unmetamorphosed Upper Devonian limestones and Lower Carboniferous flysch that is capped by wildflysch deposits (Wajsprych, 1978, 1986, 2008). The wildflysch contains large olistoliths of lower Paleozoic (Ordovician and Silurian) and Devonian deep marine sediments (Haydukiewicz, 1990). The Bardo succession was folded at the turn of the Early-Late Carboniferous into E-W–trending folds and intruded by the Kłodzko-Złoty Stok

Grzegorz Racki https://orcid.org/0000-0003-4609-8341
†racki@us.edu.pl.

GSA Bulletin; September/October 2022; v. 134; no. 9/10; p. 2373–2398; https://doi.org/10.1130/B35971.1; 18 figures; 3 tables; 1 supplemental file.
Published online 4 February 2022

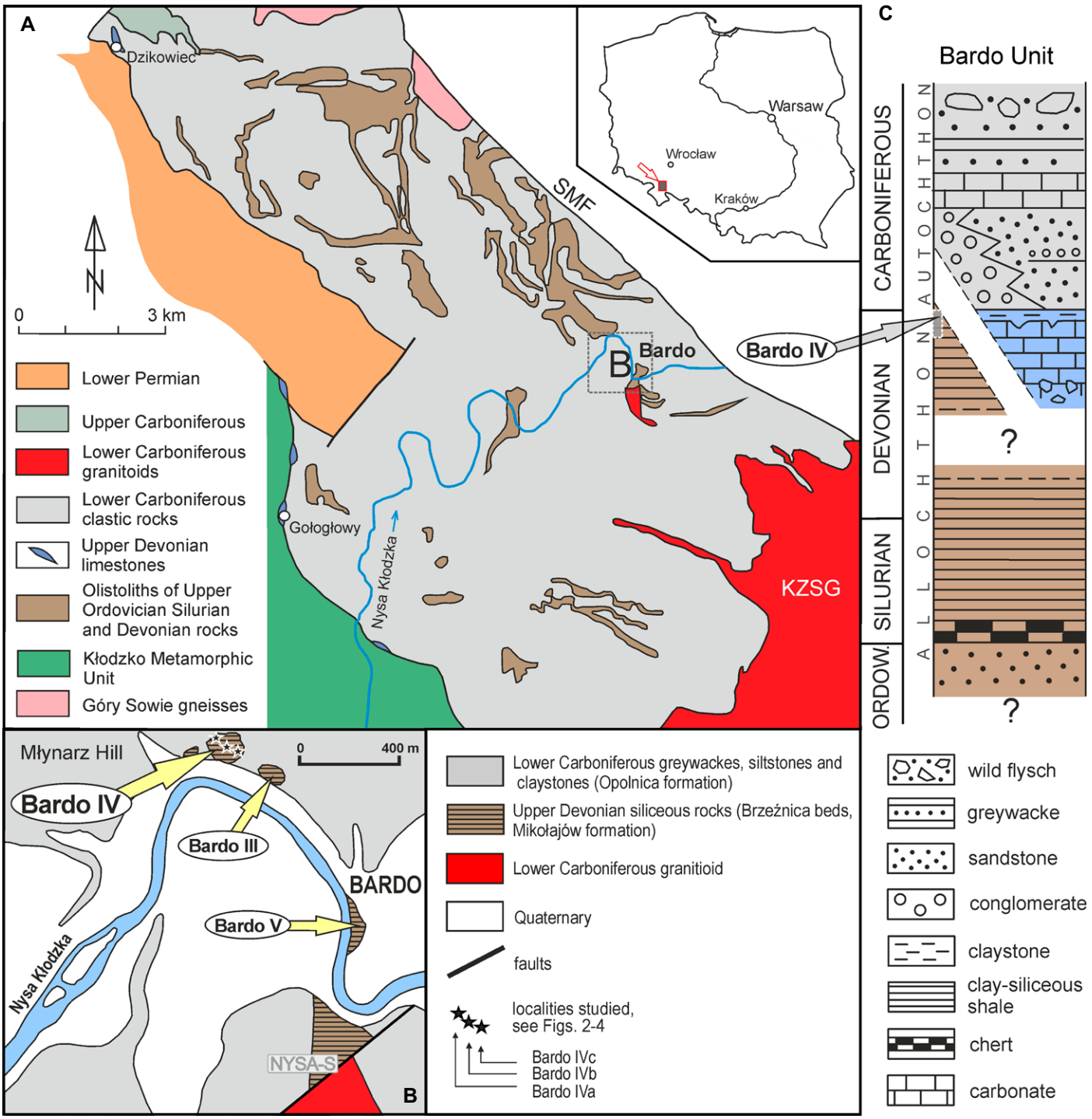

Figure 1. (A) Location geological map of the Bardo Mountains (Góry Bardzkie) within the Central Sudetes, SW Poland, with marked Bardo area (dashed box; fig. 2 from Kryza et al., 2011). (B) Geological sketch-map of Bardo vicinity based on figure 1 from Haydukiewicz (1998) (modified after Oberc et al., 1994), with arrowed studied localities Bardo III (marked by a thick dark shaly level), IV, and V (see Figs. 3 and 4), and (C) simplified lithostratigraphic column of the Bardo Sedimentary Unit after Mazur et al. (2006, their fig. 4; compare Aleksandrowski et al., 2000, their fig. 2), with arrowed studied latest Devonian interval in Figure 1C. SMF—Sudetic Marginal Fault; KZSG—Kłodzko–Złoty Stok Granitoid; Ord.—Ordovician; NYSA-S—outcrop Nysa-South.

granitoid pluton. Late Carboniferous refolding produced NE-SW to N-S–trending folds, superposed onto the older E-W structures (Oberc, 1972). From Viséan times onward, the Góry Sowie Massif supplied the marginal parts of the Bardo basin with abundant gneissic pebbles that accumulated in a system of coarse clastic fans (Wajsprych, 1978, 1986; Pacholska, 1978). The mapped relationships show that the Bardo

basin is partly floored by the Kłodzko metamorphic rocks and partly by the Nowa Ruda Ophiolite. Moreover, the only borehole that drilled through the entire Bardo succession was stopped after penetrating typical Góry Sowie gneiss (Chorowska et al., 1992).

The Middle-Late Devonian termination of folding and metamorphism in the Kłodzko Unit and the adjacent Nowa Ruda Ophiolite is constrained by an unconformity at the base of non-metamorphosed late Frasnian or earliest Famennian sediments resting on crystalline basement rocks (Bederke, 1924; Kryza et al., 1999). The most complete section of this Upper Devonian succession is exposed at Mt. Wapnica in Dzikowiec, SW Poland, adjacent to the Nowa Ruda Ophiolite (e.g., Bederke, 1924; Mazur, 1987). The unconformity that truncates the metamorphic rocks of the Kłodzko Unit and the Nowa Ruda Ophiolite, presumably developed during a relatively short time interval of ~10 m.y. between the early Givetian and late Frasnian. This is suggested by the late Frasnian-Famennian age of limestones, which directly overlie the basal conglomerates (Bederke, 1929), and by the early Givetian age of a coralline fauna from the greenschist facies crystalline limestone of the Kłodzko Unit (Hladil et al., 1999). The presence of this unconformity implies that at the transition from the Middle to the Late Devonian, freshly deformed and metamorphosed rocks had been exposed and onlapped by deposits of the Bardo Basin that eventually were folded during Namurian times (Oberc, 1972).

The Bardo Basin sedimentary series does not form any continuous stratigraphic succession. Autochthonous limestone-dominated Upper Devonian–Tournaisian pre-flysh strata (Wapnica Formation), resting on the ophiolitic gabbro (Mazur, 1987), are capped by Tournaisian black shales (Gołogłowy Formation; Haydukiewicz, 1990), and Viséan gneissic sandstones and conglomerates (Nowa Wieś Formation). The latter were deposited by high density currents and debris flows clearly derived from the Góry Sowie gneisses (Pacholska, 1978; Wajsprych, 1978). The Nowa Wieś Formation is overlain by the late Viséan to possibly Namurian clastic sequence of the Srebrna Góra Formation, composed of very proximal turbidites passing upwards into a wildflysch and olistostrome (Wajsprych, 1978, 1986, 2008). The oldest allochthonous (Zdanów-Bardo-Dębowina) succession is characterized by a transition from the flysch dominated Upper Ordovician sandstones and siltstones into hemipelagic and pelagic Silurian and Early Devonian shales (Porębska, 1982). In general, siliceous shales and cherts, with rare interbeds of thin, siliciclastic turbidites and tephras make up the Lower Silurian (Llandoverian)–Lower Devonian (Pragian) part of the pelagic allochthonous sequence (Porębska, 1982; Wyżga, 1987). The Middle to Upper Devonian rocks show a more pelitic development (claystone, argillaceous shale) with rare siliceous interbeds (Haydukiewicz, 1990; Franke et al., 1993). The affinity of the Bardo succession to the Bavarian facies of the Saxothuringian zone has been repeatedly postulated in the literature (Franke et al., 1993, 2017; Franke and Żelaźniewicz, 2000). Consequently, the investigated sediments of the Bardo Unit may represent a vestige of the sedimentary fill of the Paleozoic Saxothuringian Ocean (Franke and Żelaźniewicz, 2000; Mazur and Aleksandrowski, 2001) that was closed during accretion of the Sudetes and amalgamation of Gondwana with Laurussia. The studied chert-dominated section in the town of Bardo was later intruded by the Graniec-Bardo apophysis (341.6 ± 2.8 Ma; Mikulski and Williams, 2014), an irregular dyke sourced from the Kłodzko-Złoty Stok Granitoid Pluton, that imposed low-grade contact metamorphism and auriferous ore mineralization (Mikulski and Williams, 2014).

ANALYTICAL SECTIONS AND STRATIGRAPHIC SUCCESSION

Four outcrops, Bardo I to Bardo IV, were logged and sampled at the northern riverbank of Nysa Kłodzka, above the road from Bardo to Opolnica on the steep slopes of Młynarz Hill (412 m above sea level), during two-stage field works in May and October 2017. The map of Oberc et al. (1994) shows that overturned Devonian to Carboniferous strata, dipping at an angle of 35–65° to the NE, are exposed along this road. Only the Bardo IV site, distinguished by a tephra-bearing cherty succession, is presented in this article. Note that some Carboniferous tephras were previously studied from the northern Bardo Unit (Kryza et al., 2011); in addition, Gunia (1985; his table 3) reported "tuffite" intercalations from the Lower Devonian siliceous and clayey shales.

According to the description by Haydukiewicz (1979; p. 87–88 and p. 90–91, outcrops BoI and BoII; see also Oberc, 1957, p. 117, locality 3), the radiolarite localities were dated with conodonts as middle to late Famennian (the Famennian subages/substages, including the latest Famennian, are after Streel et al., 2000, their fig. 6; Becker et al., 2020, p. 747). However, the comparison of the lithology descriptions and conodont dating precludes any conclusive correlation with previously described localities, possibly due to changing outcropping in the steep slope area and/or renovation works along the road. Other mudstone-dominated sections provide only very scarce conodont data.

The Upper Devonian sequence at Młynarz Hill consists of claystones, siltstones, and siliceous shales, alternating with graywacke sandstone sets (Oberc et al., 1994). In regional lithostratigraphic informal terms, the strata were assigned to the "Mikołajów shales formation," overlain by the Lower Carboniferous "Opolnica formation," including exactly the same lithologies (see also Oberc, 1957, p. 116; Haydukiewicz, 1998; Cymerman et al., 2015). However, as originally defined by Oberc (1951, 1957, p. 29, 1980, their fig. 7), Mikołajów shales are typically green or yellow, thick-fissile (platy), and thinly laminated argillaceous shales. Conversely, the siliceous-shaly lithofacies was distinguished as the Brzeźnica beds, i.e., siliceous and quarzitic shales with thin intercalations of gray or green clayey shales, and rarely with partings of white "kaoline shales" (Oberc 1957, p. 30). Our observations indicate that the reconstructed cherty Famennian succession in the Bardo area (Fig. 2A) is several dozen meters thick. Hence the term "siliceous/cherty Brzeźnica beds," as a characteristic local variety of Mikołajów shales in the Brzeźnica-Bardo area, has been maintained herein (see also Haydukiewicz, 1979, p. 94–95; Oberc, 1980, their fig. 7).

Locality Bardo IV

Bardo outcrops IVa and IVb are situated on the opposite sides of a small ravine (Fig. 3A). A third site, larger, more than 20 m long locality IVc (50°30′42.40″N, 16°43′51.57″E), is located east-southeast from the IVb site. Within the composite ~8.5-m-thick succession, four faults are recognized, but the nature of the contact between similarly dipping successions IVb and IVc is uncertain owing to a concealed boundary between the two intervals.

In section IVa, a steeply dipping tight fold (Fig. 3B) exposes mostly thin layers of cherts, as well as a discontinuous thin horizon of easily weathered black shale, in places thickened up to several centimeters and shattered along the shear surface of the contrasting lithologies. The cherty strata in section IVb are less tectonized, although they are partly displaced as a result of tectonic overhangs, and likely earlier affected by disruptive mass movements (Figs. 2A and 3C). Several discontinuous tephra interbeds up to 2 cm thick are found here.

For the largest IVc locality, a composite section was made by correlating three subsections (α, β, γ), taking into account the thickness of these layers, their fabrics, superposition, and vertical distances (Figs. 2 and 4A). Despite minor tectonic deformation and sub-horizontal

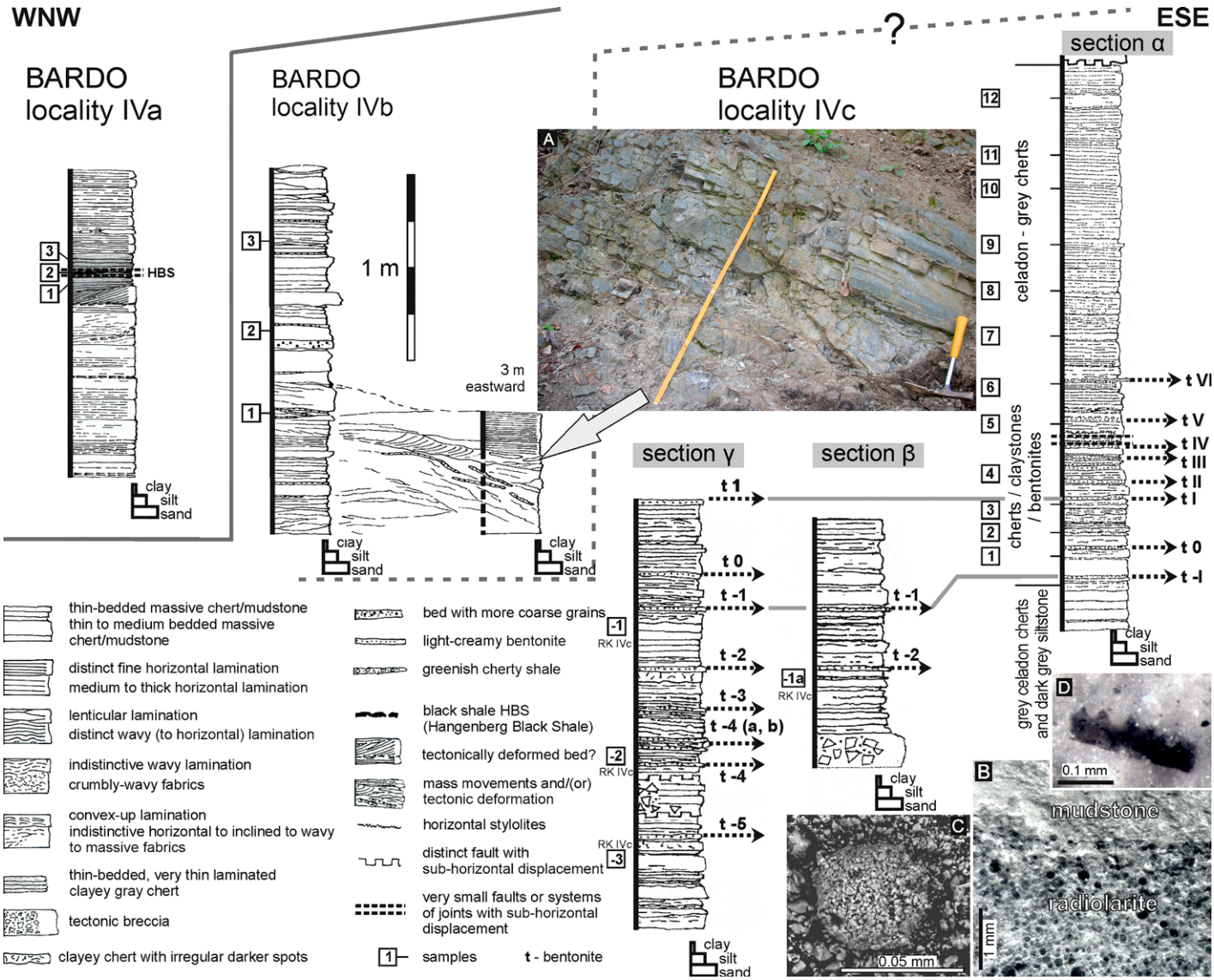

Figure 2. Columnar sections of the complex outcrop Bardo IV, near a road to the Opolnica village, SW Poland, logged in 2017 (see Figs. 1B, 3, 4A, and 4B), ordered in the succession according to field logging, i.e., in inverted order in light of biostratigraphic datings. The variation in the lamination and fabrics of layers and styles of tectonic deformation are shown, as well as soft-sediment deformation structures, in the lower conglomeratic part of section IVb (photo A). All sections are in the same vertical scale. Three examples of etched chert slabs (in HF), presented in the lower right corner, show an erosional contact of radiolarite with mudstone (sample IVc/1; B), recrystallized radiolarian(?) test (RK IVc-3; C), and a fragment of alleged graptoloid rhabdosome (RK IVc-3; D), respectively. HBS—Hangenberg Black Shale.

slip surfaces, the correlation is supported by tracing of cm-thick tephras (Fig. 4B). Mostly dark gray chert/mudstone layers are often less or more distinctly horizontally and sometimes wavy laminated. Only exceptionally, a coarser grain admixture, as well as tectonic breccias, can be recognized.

Locality Bardo V

The conodont-bearing cherty olistolith was described by Oberc (1957, locality 2) and Haydukiewicz (1998) from the northern side of the Nysa Kłodzka River cut north of a bridge in the middle of the town of Bardo (Fig. 1B). The 130-m-long exposure includes several differently oriented tectonic blocks (Fig. 4C) and wedges, a few to over a dozen meters thick, separated by tectonic breccia zones in the core of the fold (Mikulski and Williams, 2014). Dark gray radiolarite layers are ~20 cm thick, and dip 55–80° steeply northward.

The strata were dated by conodonts in the topmost Famennian (maximally, the interval of Late *expansa* to the undivided *praesulcata* zones; Haydukiewicz, 1998), which corresponds of *Bispathodus ultimus* to the earliest *Protognathodus kockeli* zonal interval in the revised zonation of Spaletta et al., 2017). The locality was only comparatively studied herein for geochemistry.

METHODS AND MATERIAL

A total of 28 samples, including six from tephras, were collected for analyses from an ~8.5-m-thick composite section of the Bardo

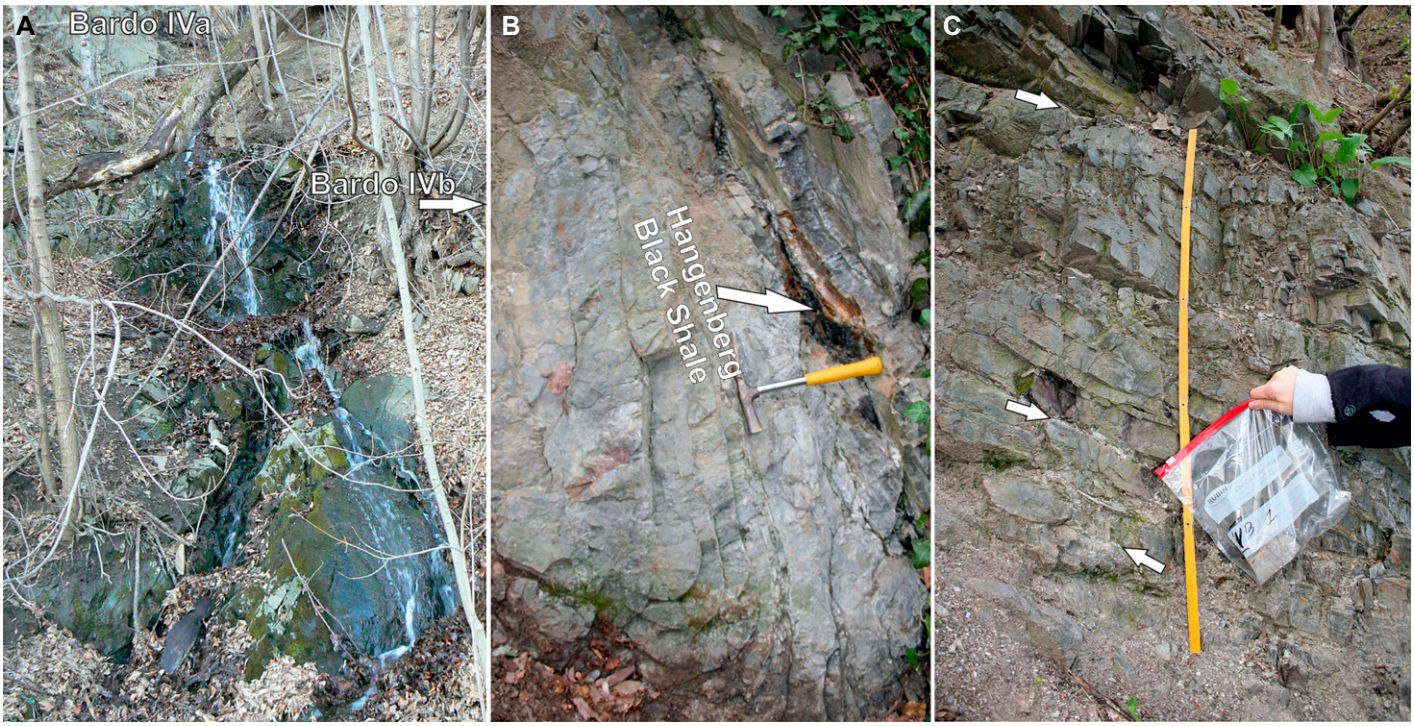

Figure 3. Bardo sections IVa (A and B) and IVb (C) at the locality of Bardo IV on Młynarz Hill in Bardo town, near the road to Opolnica village in SW Poland (see Fig. 1B). (A) General view of the Bardo IVa site at a small ravine with a persisting stream, filled mostly by deluvial till (Oberc et al., 1994). (B) Light gray-bluish, mostly thin layers of chert with almost vertical dips, converging in a downward-oriented joint of an isoclinal fold (left side) at the Bardo IVa site. Note arrowed laterally disrupted Hangenberg Black Shale that is horizon along the fault surface. (C) Light gray thin- and medium-layered cherts in the lower part of the Bardo IVb section, where the tectonic disturbance likely overlapped with previous mass movements (see Fig. 2A). Between some layers, mm-sized horizons of cream-colored tephra are visible (arrowed).

IV slope exposure (Fig. 2A), interpreted collectively as a faulted overturned succession.

Major, minor, and trace element abundances were determined on all bulk rock samples at the Acme Analytical Laboratories (Vancouver) Ltd, Canada. Total concentrations of the major oxides and several minor elements were reported from a 0.2 g sample analyzed by inductively coupled plasma (ICP)-emission spectrometry following lithium metaborate/tetraborate fusion and dilute nitric acid digestion. Rare earth and refractory elements (e.g., Ba, Co, Th, U, V, Zr) were determined by ICP mass spectrometry (MS) following the same decomposition method. A separate 0.5 g split was digested with 3 ml 2:2:2 HCl-HNO_3-H_2O and also analyzed by ICP-MS for the precious and base metals (e.g., Mo, Cu, Pb, Zn, Ni, As, Sb). In addition, total carbon and sulfur were analyzed by Leco. The reliability of the data was checked by analyses of international standard reference materials. Precision and accuracy of the results were better than ±0.9% (mostly ±0.4%) for the 11 major elements, and better than ±15% for the 45 trace elements. When the concentrations of trace metals (especially Hg, Cd, As, and Mo) were lower than the detection limits (see Supplemental Material S3[1]), the highest value below the suitable detection limit value was used. Mercury concentrations were determined using a two-cell, pyrolyzer-type Milestone DMA-80 direct mercury analyzer for atomic absorption spectrometry (AAS) at the Institute of Earth Sciences, University of Silesia (Poland). For analytical details see Racki et al. (2018).

The 18 cherty samples were macerated for radiolarians and bioapatites in hydrofluoric acid. The material was obtained by digestion of 50–70 g pieces with a 5% HF solution for 24 h. Th residuum was wet sieved through 57 μm and 430 μm sieves. Two samples from the black shale horizon from Bardo IVa section were selected for the palynological investigation. Standard laboratory procedure was employed (HCl-HF-HCl acid sequence; Wood et al., 1996). Rich organic remains, including miospores, phytoplankton taxa, and other palynomorphs, were obtained and sieved through an 18 μm nylon mesh. Finally, 10 standard palynological slides were prepared. Peropoxy 154 was used as a mounting agent; Cellosize was used as a dispersal agent to avoid organic clumping. Examination and documentation were done using a Nikon Eclipse 50*i* transmitted light microscope with a DS-U3 controller and Nikon NIS-Elements imaging software suite. The micropaleontological collections of conodonts and palynomorphs are housed at the Department of Natural Sciences (University of Silesia, Sosnowiec, Poland).

Laser ablation (LA)-ICP-MS U-Pb dating of zircons from three tephra samples was carried out at the Institute of Geochemistry and Petrology, ETH Zürich, Switzerland. The analytical methods followed Guillong et al. (2014); all details of instrumental setup and results are provided in Supplemental Material S2.

[1]Supplemental Material. Supplemental Material S1: Conodont alteration index discussion; Supplemental Material S2: Radioisotopic data; Supplemental Material S3: Geochemical analytical and correlation dataset; Supplemental Material S4: Additional geochemical figures. Please visit https://doi.org/10.1130/GSAB.S.17149046 to access the supplemental material, and contact editing@geosociety.org with any questions.

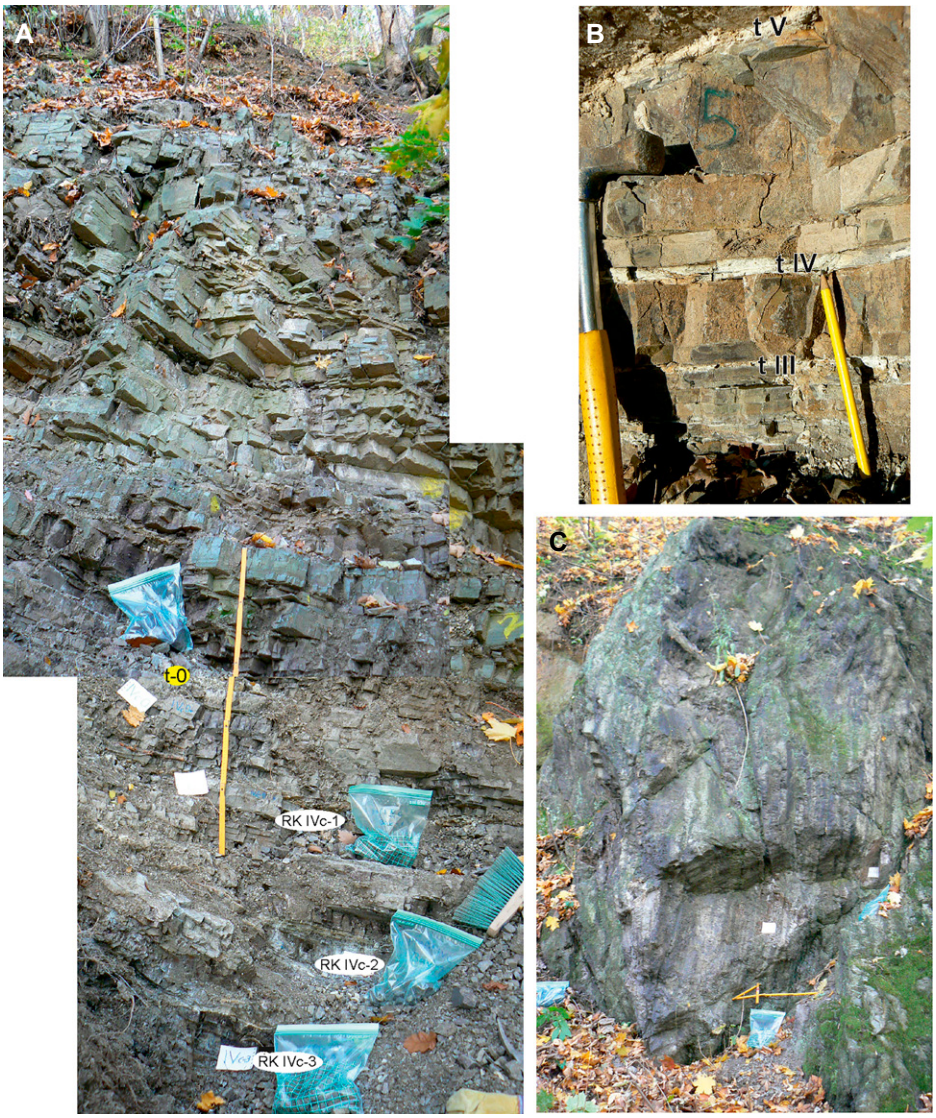

Figure 4. Reference section Bardo IVc on Młynarz Hill in Bardo town, near the road to Opolnica village in SW Poland (A and B; see Figs. 1B and 2A), encompassing inverted cherty-clayey succession, and the auxiliary of locality Bardo V (C), in the middle of Bardo town. Some sampled horizons are shown. (A) A series of thin-layered, gray mudstones and siliceous shales succeed upwards into thin- and medium-layered, horizontally laminated cherts of the subsection IVc-β. Horizontal tectonic displacements along the surface of the cherty layers are recorded in thin layer splits (siliceous shale habitus; compare lithofacies 1 in Fraser and Hutchison, 2017). Tephra partings (see Fig. 4B) characterize the lower and middle part of the section. (B) Cream-colored tephras, up to 2 cm thick, between the secondarily brownish, differently layered cherts in the middle of the IVc-α section (see Fig. 2A). (C) Rock promontory protruding from the cliff edge toward the Nysa Kłodzka River in the central part of the Bardo V outcrop. The succession comprises steeply dipping end-Famennian cherts (see the Block III in Haydukiewicz, 1998, their fig. 4).

BIOSTRATIGRAPHY

Two important microfossil groups, conodonts and palynomorphs, were recovered from the siliceous-clayey deposits from the Bardo IV site. Unfortunately, the poorly-preserved spherical spongy tests of polycystine radiolarians of the family Entactinidae (Fig. 2C) were not useful from a biostratigraphical point of view.

Conodonts

The conodont collection studied includes 175 P_1 elements found in 11 samples from the Bardo IVc and IVb sites (Table 1). The very fragile elements are mostly broken, fractured, deformed, and corroded, and the best preserved are juvenile and early juvenile individuals, comprising 60% of the collection investigated. The frequency of elements in the samples is low, not exceeding 30 specimens per sample, which precludes quantitative biofacies analysis. Nevertheless, *Palmatolepis* (*Pa.*) is the dominant genus, attaining 84% and 73% of total number of specimens in the Bardo IVc and Bardo IVb sections, respectively.

In all samples investigated the conodont color alteration index (CAI) has been determined, based on the reference material kindly supplied by Anita Harris (U.S. Geological Survey), and on the Rejebian et al. (1987) color scale. The elements are generally gray in color with white denticle terminations, which points to CAI 6 values corresponding to temperatures of 360–550 °C (Supplemental Material S1). Single assemblages display higher values, up to CAI 7, thus indicating temperatures >600 °C. Such high temperatures and lateral CAI variability show that the host sediments had been heated during the contact metamorphic processes (Haydukiewicz, 2002), probably related to a hidden small apophyse related to the Kłodzko-Złoty Stok granitoids (Mikulski and Williams, 2014).

The investigated collection includes 11 species and subspecies (Table 1; Fig. 5). In view of partly missing zonal indicators, the biostratigraphy of particular samples was based on comparison of total ranges of possibly all co-occurring taxa, referred to the zonation proposed by Spalletta et al. (2017). In the Bardo IVc section, the interval from sample IVc/12 to IVc/1 corresponds with *Pa. marginifera* to *Pa. marginifera utahensis* (Table 1). This is based on the presence of *Pa. m. marginifera* in sample IVc/12 (Fig. 5: see no. 17) and *Palmatolepis glabra prima* (Fig. 5: see no. 3) in sample IVc/1. The lower age limit is defined by *Pa. m. marginifera*, being the index taxon for the *Pa. m. marginifera* Zone. The upper limit is defined by the last appearance (LAD) of the subspecies *Pa. glabra prima* (see Spalletta et al., 2017). Very poor material from locality IVb allows the dating of the middle Famennian (*Pa. m. marginifera* to *Pa. m. utahensis* zones). The age was constrained by the presence of *Branmehla werneri* (Fig. 5: see no. 23) that has a first appearance datum in the *Pa. m. marginifera* Zone, and the LAD of *Pa. glabra prima* (Fig. 5: see no. 6). In summary, the conodont faunas document a middle Famennian sequence in the Bardo IVb-IVc succession (Fig. 2).

Conodont assemblages from single samples from Bardo II and III sites (Fig. 1B) are poorer

TABLE 1. CONODONT DISTRIBUTION IN SAMPLES FROM SECTIONS BARDO IVC AND IVB (SEE FIG. 2A)

Sections	IVc										IVb
Conodont zones	*Pa. marginifera marginifera–Pa. marginifera utahensis*										
Sample numbers	12	11	10	9	7	5	4	3	2	1	1
Palmatolepis marg. cf. *marginifera*	2	1		2							
Palmatolepis glabra pectinata	4	6	2	1							
Palmatolepis glabra prima	1				1	3		3	5		1
Palmatolepis glabra cf. *prima*										1	
Palmatolepis glabra	3	3	1	1			4				
Palmatolepis gracilis gracilis		2			4	6	6	1	4	2	1
Palmatolepis gracilis cf. *gracilis*	3	1				5	4				
Palmatolepis gracilis semisigmoidalis								1			
Palmatolepis gracilis						2	1	1	9	7	3
Branmehla werneri		1						2		1	2
Branmehla cf. *werneri*						2	2	3	1		
Branmehla sp.		2			1	5	2				
Palmatolepis perlobata schindewolfi								1	1		
Palmatolepis perlobata								1			1
"*Polygnathus*" *diversus*							1		3		1
Palmatolepis sp.			1	1	2	5	7	1	7	4	2
Pandorinellina sp.						2	1	1			
Belodella sp.								1			
Ramiforms	8	4	1	2	7	22	18	6	35	15	29
Total P_1	13	16	4	5	8	30	28	15	30	15	11

Note: *Pa*.—*Palmatolepis*.

than those from the Bardo IV section. They point to the occurrence of an undivided interval from the middle Famennian (*Palmatolepis gracilis gracilis* Zone) to the early Tournaisian (*Protognathodus kockeli* Zone).

Palynomorphs

All organic matter (OM) from the Bardo IVa/2 samples was significantly changed under the influence of high temperature and is black in color (Fig. 6). Moreover, palynomorphs are frequently cracked, with signs of recrystallization.

Among some taxa classified as miospores, there are specimens with visible central bodies and an external perispore layer with characteristic reticulate ornamentation. Such features are particularly characteristic of *Retispora lepidophyta,* the guide species occurring only in the latest Famennian (see Streel et al., 1987, 2000; Higgs et al., 1988). Its disappearance is treated worldwide as the marker for the Devonian-Carboniferous (D-C) boundary. In the studied material, smaller forms are dominant, which should be classified as *R. lepidophyta* var. *minor*. The larger variety, belonging to *R. lepidophyta* var. *lepidophyta* (see Maziane et al., 2002) are present less frequently. It should be stressed, however, that even if the palynomorphs, identified here as ?*R. lepidophyta* (Fig. 6: see nos. 1–8), are only dubiously attributed to this species, this taxonomic interpretation is strengthened by the occurrence of the guide species in the Hangenberg Black Shale (HBS) in another D-C boundary section in the Bardo Unit (Wapnica quarry at Dzikowiec village in Kłodzko County, Matyja et al., 2021; Fig. 6: see nos. 22–25). Other miospores are similar to *Grandispora*?, *Tumulispora*?, and *Vallatisporites*?, frequent palynofloral components for a broader D-C transition interval. They quantitatively predominate over ?*R. lepidophyta*.

Acritarchs are quite common and represented by dominantly spherical forms, variably equipped with long, narrow appendages or possessing shorter spines. From known species, *Gorgonisphaeridium* possess this type of architecture. Some taxa are similar to *Gorgonisphaeridium ohioense* (Fig. 6: see nos. 14 and 20) from the Late Devonian (Wicander, 1974; Le Hérissé et al., 2000). Other forms with smaller ornamentation sometimes possess additionally partial rupture characteristic of *Lophosphaeridium* (Fig. 6: see no. 13).

The beginning of the Carboniferous was a time where a significant phytoplankton crisis is noted, a so called phytoplankton blackout (*sensu* Riegel, 2008; Martin and Servais, 2019). Therefore, *?Retispora lepidophyta* and spherical acritarcha have significance for supporting the latest Famennian age of the assumed HBS level. Moreover, the co-occurrence of miospore tetrads (Fig. 6: see nos. 9 and 10) may also be significant here, and at Dzikowiec (Matyja et al., 2021). The higher miospore concentration was previously noticed in the topmost Devonian (European standard lepidophyta–nitidus (LN) Miospore Zone) from the Kowala Quarry (Filipiak and Racki, 2010), and other regions (Prestianni et al., 2016; Marshall et al., 2020).

ZIRCON GEOCHRONOLOGY OF TEPHRA HORIZONS

Three tephra (t) samples from the Bardo IVc section yielded pristine, euhedral zircons of presumed volcanic origin (see Supplemental Material S2). Individual LA-ICP-MS $^{206}Pb/^{238}U$ zircon dates range from 378 to 349 Ma, with a single crystal at 549 Ma (sample t IV) and one crystal at 337 Ma (t III) that likely records partial Pb loss (Fig. 7). Weighted mean $^{206}Pb/^{238}U$ ages are indistinguishable between the three samples at 360.3 ± 3.8 Ma (t II), 362.7 ± 4.0 Ma (t III), and 360.7 ± 4.0 Ma (t IV). Given the euhedral nature of the dated zircons and their simple (if over dispersed) age distributions, we interpret the results as primary magmatic crystallization ages. The ages indicate that the tephras of the lower half of the Bardo IVc section are products of later Famennian volcanism.

STRATIGRAPHIC SUCCESSION AND THE QUESTION OF THE HANGENBERG GLOBAL EVENT

Summarizing the biostratigraphic dating correlations provided by conodonts (sections IVb and IVc) and palynomorphs (IVa), it is possible to consistently interpret the faulted Bardo succession (Fig. 2), corresponding to the cartographic setting provided by Oberc et al. (1994). The middle Famennian age of the topographically higher part of section IVc documents the bottom part of an overturned succession (Fig. 8), in agreement with dating of BoI locality (claystones of the Mikołajów shales) by Haydukiewicz (1979). In the west, the slice has a contact with the tectonized block IVa, tentatively assigned using palynomorphs to the latest Famennian *Retispora lepidophyta* Palynozone. Thus, the distinctive black shale intercalation is thought herein as the Hangenberg Black Shale.

The radiometrically dated (360.7–362.7 ± 4.0 Ma) tephras come from the conodont-dated middle Famennian interval, which would correspond to between 367.3 and 363.4 Ma following the astronomical time calibration of Ma et al. (2020, their fig. 8). The partly overlapping ages are confirmation of the age interpretation, especially given that the geochronology of Famennian biozones is still uncertain (compare dates in Becker et al., 2020). In light of conodont data presented by Haydukiewicz (1998), the additional Bardo V succession (Fig. 1B) probably corresponds to a tectonic gap in the thrust separating Bardo IVa and IVb sections (see Figs. 2 and 8). All the data suggest a significant primary thickness of the cherty Brzeźnica beds.

MICROFACIES OF CHERTY LITHOLOGIES

The siliceous rocks of the Bardo IVc section are composed of monotonously textured microcrystalline quartz with an admixture of other silicates. Biotic components are rare and largely limited to radiolarians and palynomorphs, the

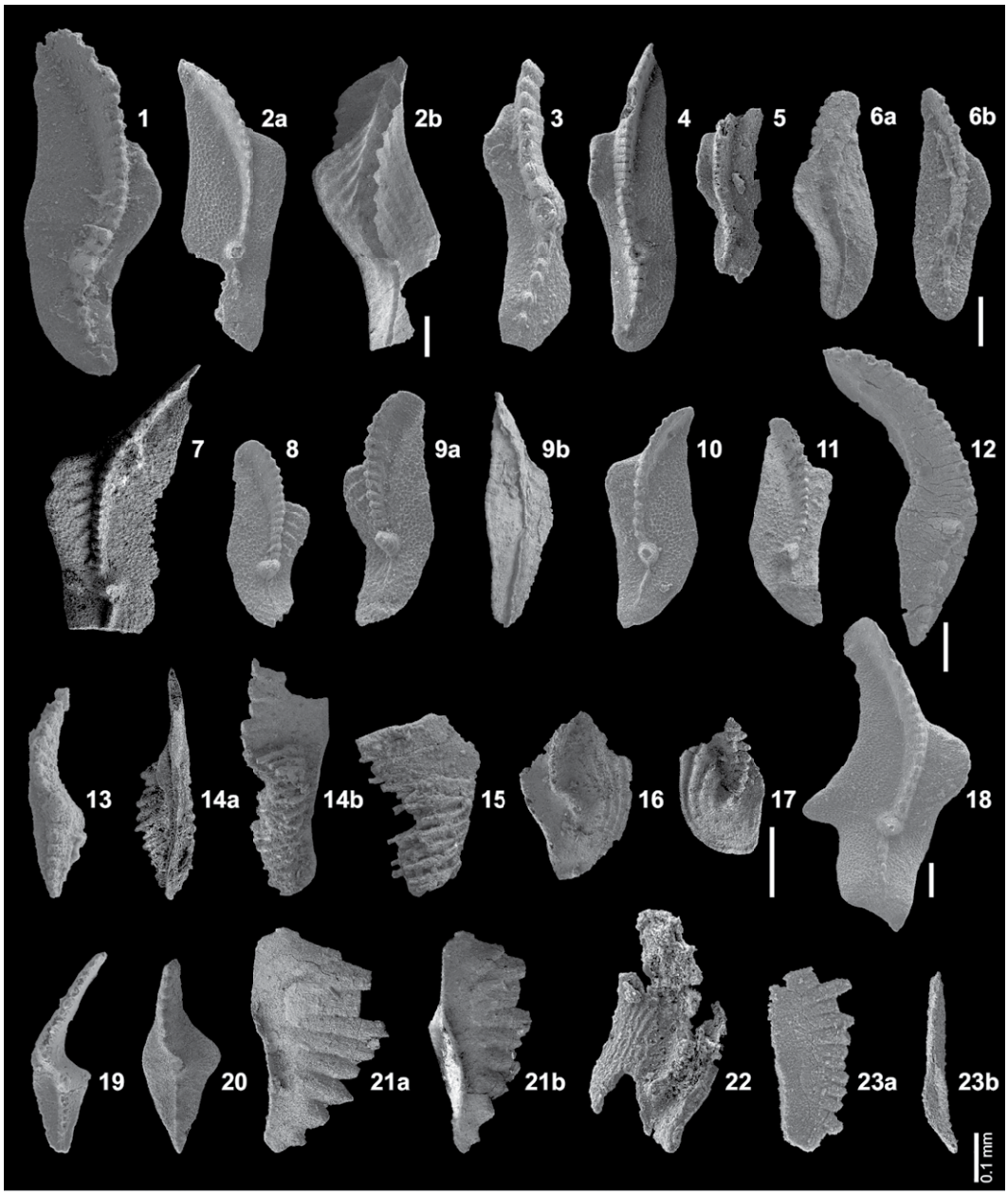

Figure 5. Conodont elements from the Bardo IV section (IVc and IVb; Table 1). 1, 2, and 6–11: *Palmatolepis glabra prima* Ziegler and Huddle (1969) (1—upper view, sample IVc/2, GIUS 4-3737/1; 2a—upper view; 2b—lower view, IVc/5, GIUS 4-3737/3; 6a—lower view; 6b—upper view, IVb/1, GIUS 4-3737/20; 7—upper view, IVc/12, GIUS 4-3737/6; 8—upper view, IVc/3, GIUS 4-3737/7; 9a—upper view; 9b—lower view, IVc/5, GIUS 4-3737/8; 10—upper view, IVc/5, GIUS 4-3737/4; 11—upper view, IVc/2, GIUS 4-3737/5). 3: *Palmatolepis glabra* cf. *prima* Ziegler and Huddle (1969) upper view, IVc/1, GIUS 4-3737/2. 4 and 5: *Palmatolepis glabra pectinata* Ziegler (1962) (4—upper view, IVc/12, GIUS 4-3737/9; 5—upper view of juvenile form, IVc/9, GIUS 4-3737/10). 12, 13, and 20: *Palmatolepis gracilis* Branson and Mehl (1934) (12—upper/oblique view, IVc/1, GIUS 4-3737/12; 13—upper view, IVb/1, GIUS 4-3737/21; 20—upper view, IVc/7, GIUS 4-3737/13). 14 and 15: "*Polygnathus*" *diversus* Helms (1959) (14a—lower view; 14b—lateral view of juvenile form, IVc/2, GIUS 4-3737/18; 15—lateral view of juvenile form, IVb/1, GIUS 4-3737/22). 16, 17, and 22: *Palmatolepis marginifera* cf. *marginifera* Helms (1959) (16—upper view of juvenile form, IVc/9, GIUS 4-3737/15; 17—upper view of juvenile form, IVc/12, GIUS 4-3737/16; 22—upper view, IVc/9, GIUS 4-3737/17). 18: *Palmatolepis perlobata schindewolfi* Müller (1956) (upper view, IVc/3, GIUS 4-3737/11). 19: *Palmatolepis gracilis semisigmoidalis* Hartenfels (2011) (upper view, IVc/3, GIUS 4-3737/14). 21 and 23: *Branmehla werneri* Ziegler (1962) (21a—lateral view; 21b—lateral/oblique view, IVc/11, GIUS 4-3737/19; 23a—lateral view; 23b—lower view of juvenile specimen, IVb/1, GIUS 4-3737/23). Linear scale = 0.1 mm.

latter represented mostly by acritarch-like remnants. Radiolarian tests vary between 50 and 180 μm and are mostly dissolved, replaced by quartz and preserved as mold casts (Figs. 2B–2C and 9). In addition, problematic microfossils resembling degraded planktonic unicellular algae are noteworthy (Fig. 9C).

Among microfacies, the most common variety is radiolarian chert, grading into argillaceous varieties (see below), in places with peloid-like structures. Amorphous OM is dispersed throughout the chert matrix. Dark brown "clumps" of irregular shape (sized from 20 to 200 μm), as well as pyrite grains (Fig. 9D), are abundant in some levels (Fig. 9E). Clumps composed of cryptocrystalline quartz and amorphous OM. Subordinately, especially in the lower part of Bardo IVc section, a variety with rare radiolarians occurs (Figs. 9I and 9J), in which laminations of highly disintegrated OM are rarely recognizable.

Lamination is finely developed, mostly in clay-enriched lithologies. Quartz and silicate-enriched horizons with indistinct laminae up to 500 μm thick that contain alloclasts are visible, and rarely paired with continuous and wavy organic matter streaks (Figs. 9A–9B, and 9G–9I). The presence of microbial mats is sporadically suggested, but no morphologi-

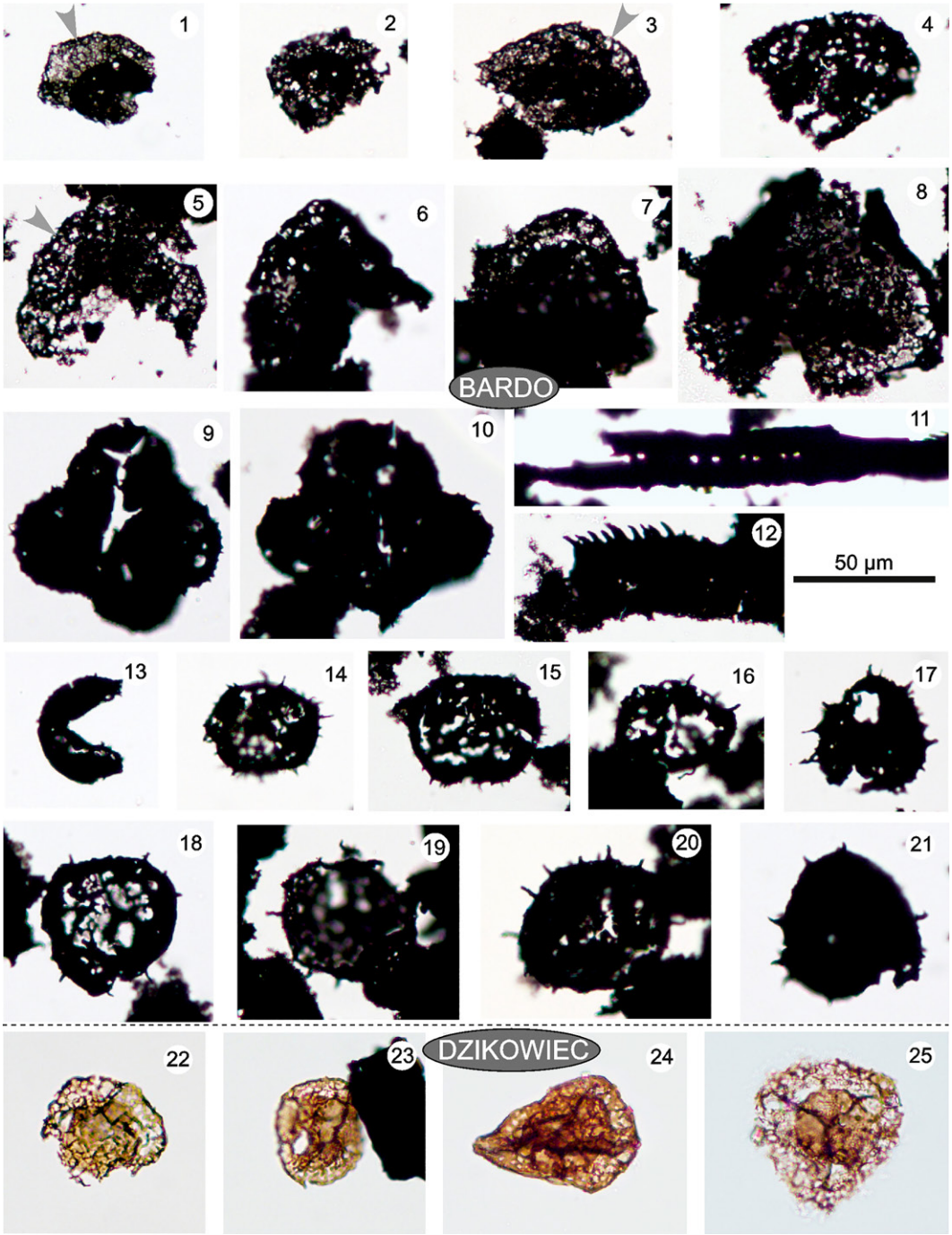

Figure 6. Palynomorphs from the Bardo IVa section (1–21; IVa-2/1 sample) and, for comparison, better preserved specimens from the Wapnica Quarry near the village of Dzikowiec, SW Poland (see Matyja et. al., 2021; 22–25). All pictures possess the same magnification. 1–4: Miospores classified as ?*Retispora lepidophyta* var. *minor* Kedo (1974) (1—best preserved specimen with partly well-preserved external perispore layer, with characteristic reticulate ornamentation (arrowed). 5–8: Miospores classified as ?*Retispora lepidophyta* var. *lepidophyta* (Kedo) Playford (1976). 9–10: Miospores tetrads. 11: Higher plant tracheid. 12: Scolecodont. 13: Acritarcha similar to *Lophosphaeridium*. 14–20: *Gorgonisphaeridium* type of acritarcha, 14 and 20: ?*Gorgonisphaeridium ohioense* Winslow (1962) and Wicander (1974). 21: Acritarcha or *Grandispora*? 22 and 23: *Retispora lepidophyta* var. *minor* Kedo (1974), sample 9. 24 and 25: *Retispora lepidophyta* var. *lepidophyta* (Kedo) Playford, (1976), sample 11.

cally preserved remnants of bacteria are visible. Therefore, the laminated organic material may have been derived directly from the water column. The absence of benthic skeletal fauna, even silicisponges, and microbial mats suggests a harsh, mostly poorly oxygenated and/or extremely muddy near-bottom habitat. The origin of the "clumps" is unclear, as they may represent highly degraded planktonic OM or some reworked sediment with benthic microbial life. Fossil excreta of a soft-bodied infauna is not supported.

PALYNOFACIES OF THE HANGENBERG BLACK SHALE

The organic material (Fig. 6) consists of diverse miospores, acritarchs, prasinophyta, higher plants tracheids, scolecodonts, and amorphic organic matter. The dominance of black amorphic OM over other organic components is typical of low-oxygen regimes in the bottom zone (Batten, 1996).

The mixed playnomorph assemblage, partly of marine (acritarchs) and land (miospores) origin, indicates a full-marine setting with a significant supply of terrestrial organic material during the Hangenberg clayey deposition. In particular, *R. lepidophyta* characterized the cosmopolitan vegetation of coastal lowlands, the downstream

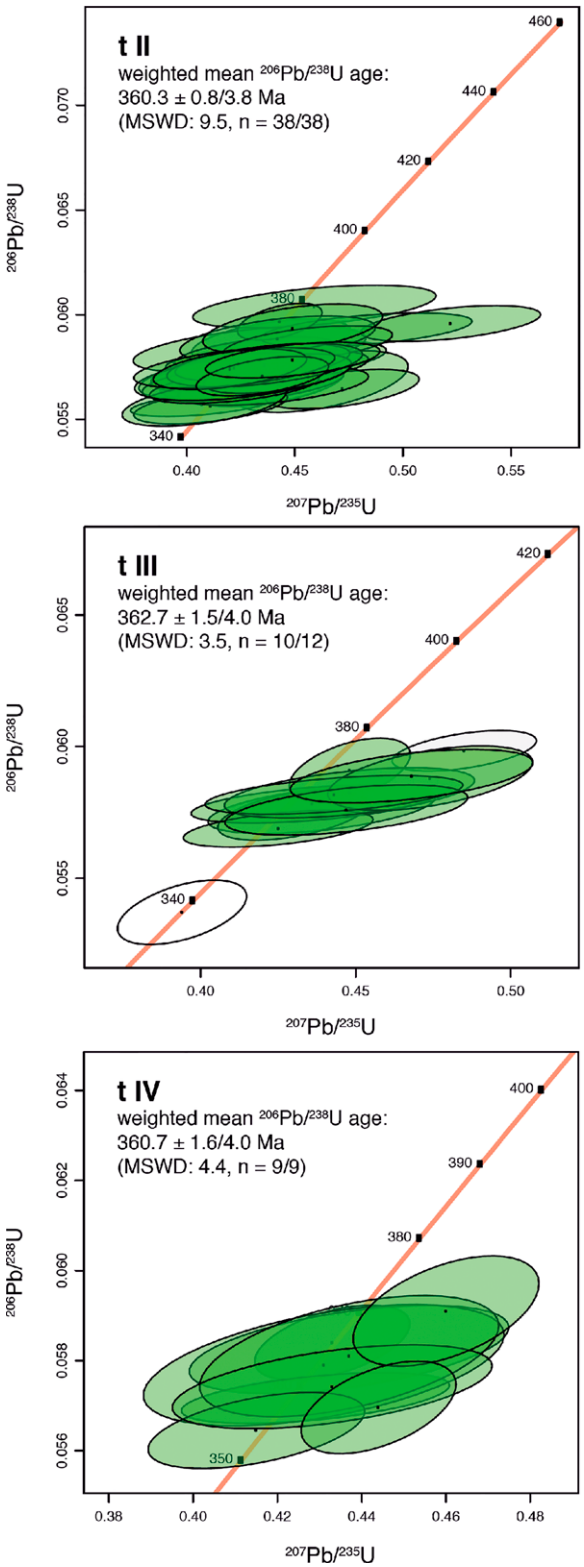

Figure 7. U-Pb zircon ages in three Bardo IVc tephra horizons of SW Poland (see Fig. 4B; for detail see DR2). Uncertainties on weighted mean ages displayed as internal/internal + 1% propagated systematic uncertainty. MSWD—mean squared weighted deviation; t—tephra.

"coal" swamp margin milieu of Streel et al. (2000, their figs. 28 and 33). Here, in addition to local humidity and equable climate, the highly effective reproduction was directly controlled by short-term sea-level fluctuations. Transgressive pulses, notable in the interglacial HBS episode (Kaiser et al., 2016), led to a rise of the freshwater table in these habitats and the expansion of marsh flora, and thus a widespread dispersal of the miospores in adjoining basins (Streel et al., 2000, p. 149).

ELEMENTAL GEOCHEMISTRY OF CHERTY ROCKS

The chemostratigraphic study of the siliceous-clayey succession Bardo IV is based on conventional analyses of whole-rock bulk samples, which is the current research standard in sedimentary geology (see reviews in Sageman and Lyons, 2003; Calvert and Pedersen, 2007; Rothwell and Croudace, 2015; Yudovich and Ketris, 2015; Craigie, 2018). The elemental geochemistry of cherts is focused on lithogenous (detrital) and non-silicate authigenic phases, strongly diluted by biogenic opal (see Murray, 1994; Sageman and Lyons, 2003). Consequently, the elemental multiproxy approach is routinely used to reconstruct environmental factors during deposition of the bedded cherts (Figs. 10–13), as exemplified recently by Kuroda et al. (2015), Ran et al. (2015), Udchachon et al. (2017), Zong et al. (2016), Fraser and Hutchison (2017), Harris et al. (2018), Dong et al. (2018), Khan et al. (2019), Gao et al. (2021), and Hou et al. (2021). Four "chemo-intervals" I–IV are distinguished in the Bardo IV succession (see below), and the black shale (sample IVa/2 = interval IV-H; Figs. 11 and 12) is summarized separately due to its many disparate characters.

To compare elemental contents and ratios in sediments with fluctuating silica dilution and detrital input, we use Al-normalization (E/Al) and enrichment factors ($E_{EF} = E/Al_{(sample)}/E/Al_{(standard)}$; Tribovillard et al., 2006; Fraser and Hutchison, 2017), in which E represents the targeted element. The average shale of Wedepohl (1971; Fig. 10A) is taken as standard. As complementary tracers of bioproductivity, the biogenic excess is calculated (Tribovillard et al., 2006; Harris et al., 2018; Dong et al., 2018) using the formula: E_{BIO} (as presented in the quoted articles; E_{EF} equivalent above) = $E_{sample} - [Al\ sample \times E/Al_{(standard)}]$. Spearman's rank correlation coefficient (r_s) is applied in the study (see Supplemental Material S3).

General Characteristics

As indicated by Jones and Murchey (1986), the term "bedded chert" or "radiolarian chert" commonly denotes rock units that include both chert and related clayey varieties (see also De Wever et al., 2001, p. 65–70; Hüneke and Henrich, 2011), which closely match the character of the siliceous rocks from Bardo. In the binomial system for classifying fine-grained siliceous sedimentary rocks of Jones and Murchey (1986), the rocks represent mainly argillaceous chert, with gradation to siliceous mudstone. "Pure" radiolarian cherts (less than 25% clay content)

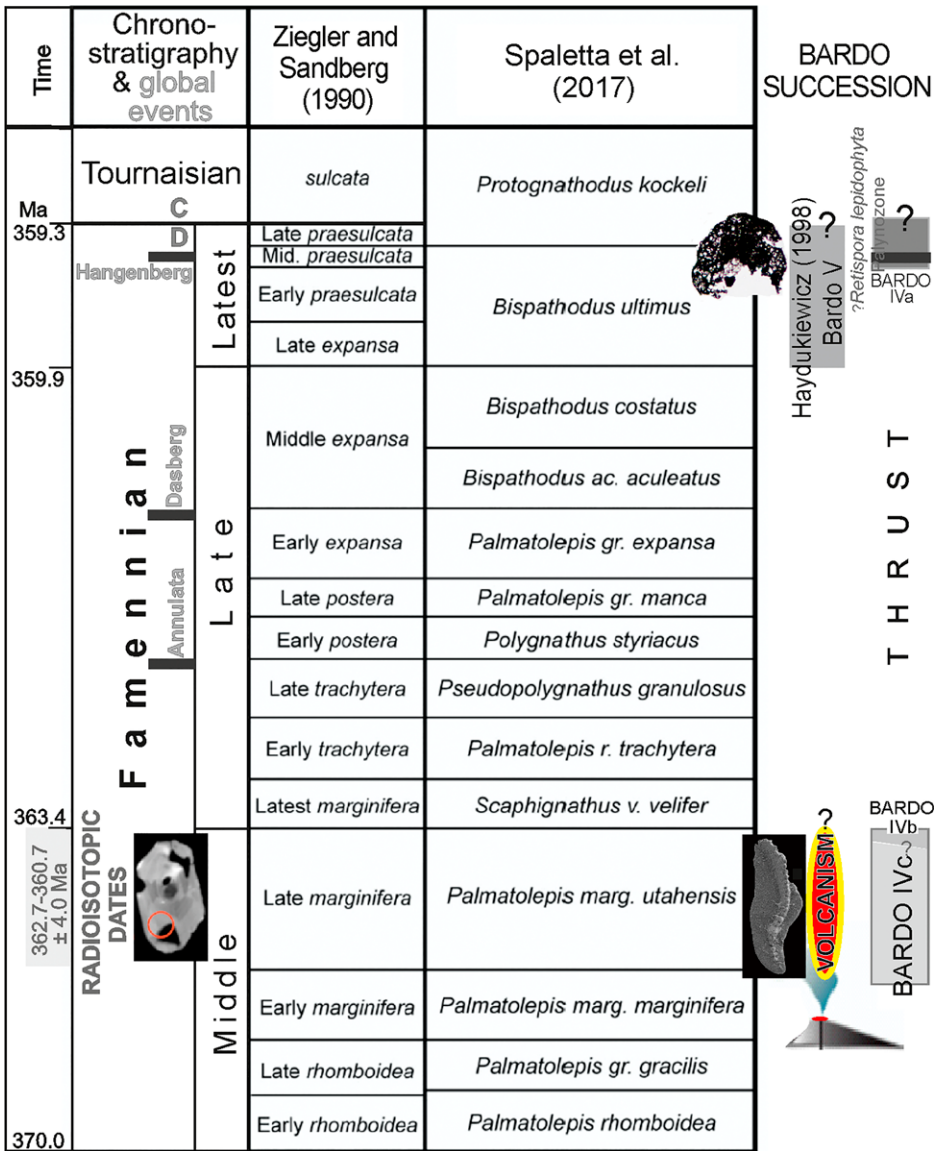

Figure 8. Geochronology, chronostratigraphy, and standard conodont zones of the middle Famennian to Early Carboniferous time, after Spaletta et al. (2017, their fig. 1; timing after Ma et al., 2020, their fig. 7, compare Becker et al., 2020, their fig. 22.11; Famennian subages after Streel et al., 2000, their fig. 6), as a reference for conodont and radioisotopic dating of the sections Bardo IV and V of SW Poland (see Figs. 1B, 2A, 7, 11, and 12; Table 1).

are likely absent at Bardo, and at least one sample (IVc/2) is a mudstone (Fig. 11).

In terms of chemical composition (see Supplemental Material S3; Table 2), the Bardo cherty succession is generally uniform. The cherts have high contents of SiO_2 (71.08%–89.66%, median 81.26%), and moderate contents of Al_2O_3 (5.11%–13.49%, median 7.63%) and Fe_2O_3 (1.76%–5.26%, median 3.02%). These deposits are impoverished in CaO (0.2%–2.76%, median 0.49%), and poor in OM, where total organic carbon (TOC) values are below 0.2% (median 0.09%).

When compared with the geochemical standards, especially with average cherty shale of Ketris and Yudovich (2009), the chert samples from Bardo display some notable depletions, especially in As, Mo, Cd, U, Sb, and Hg (Table 2). Only Mn appears enriched, even if other standards reveal similar abundances. It is not surprising that Bavarian and Sudetic radiolarian cherts show closer geochemical compatibility. The impoverishment of As, Hg, Sb, and Mo, as well as authigenic Mn enrichment is confirmed by calculated enrichment/depletion factors, but most elements follow roughly average estimates (Fig. 10A). The pattern indicates that source rocks delivered to the oceanic basin had affinity to typical upper continental crust (see below).

The total rare earth element (REE) and Y contents (ΣREE + Y) are in the range of 21.6 to 483.3 ppm (median 71.8 ppm; Fig. S4/1). The light (L)REE (15.1–325.9 ppm, median 55.9 ppm) abundance is higher than middle REE (1.5–36.0, median 4.4 ppm) and high (H) REE (1.2–23.2 ppm, median 2.7 ppm), with $(La/Yb)_N$ values near 1 (0.48–1.51, median 0.95). The cherts are characterized by average values of the Eu anomaly and Ce anomaly (defined by the equation Eu/Eu* (* is the expected normalized concentration when interpolated from an appropriate combination of near REE neighbors)= $Eu_n/(Sm_n+Gd_n)^{0.5}$, and $Ce/Ce^* = 2 \times Ce_n/(La_n+Pr_n)$, where the subscript "n" indicates REE normalization to PAAS values) ~1.1 (0.89–1.59, median 1.12 and 0.98–1.24, median 1.11, respectively).

Origin of Silica and Diagenetic Overprint

The key biogenic component of radiolarian cherts was composed originally of unstable amorphous opal A, and the tests are very poorly preserved in the studied sediments (Figs. 2C and 9F), an indication of significant solution and reprecipitation of SiO_2 during diagenetic processes (Murray et al., 1992; De Wever et al., 2001, p. 55–60; Lazarus et al., 2020, p. 218–224). The Si/(Si + Fe + Al + Ca) ratio varies between 0.76 and 0.91, which reflects the content of silica in relation to aluminosilicate phase, and ferruginous and calcareous minerals (Ran et al., 2015; Khan et al., 2019). The maximum proportion of excessive biogenic silica ranges from 11.1 to 33.6% (median 25.6%), while the admixture of clay exceeds 50% in three intervals, especially in the basal I-B slice, in which only siliceous mudstones to mudstones predominate (Fig. 11).

A covariation between the approximated biosilica content and bioproductivity proxies is also expected for radiolarites (Lei et al., 2019). The positive relationship with biophile trace metals is weak ($r_s = 0.24$ for Pb), but a more significant link is shown by biogenic P ($r_s = 0.48$). In summary, these data all support a dominantly biogenic origin of the studied cherts (see discussion in Lei et al., 2019), with an insignificant hydrothermal silica contribution (compare the jasper case in Grenne and Slack, 2005).

The essential diagenetic overprint is emphasized by Murray et al. (1992) and Murray (1994) as a leading feature of bedded chert originating from opaline-clayey muds to lithified quartz-dominated rocks, with large-scale geochemical

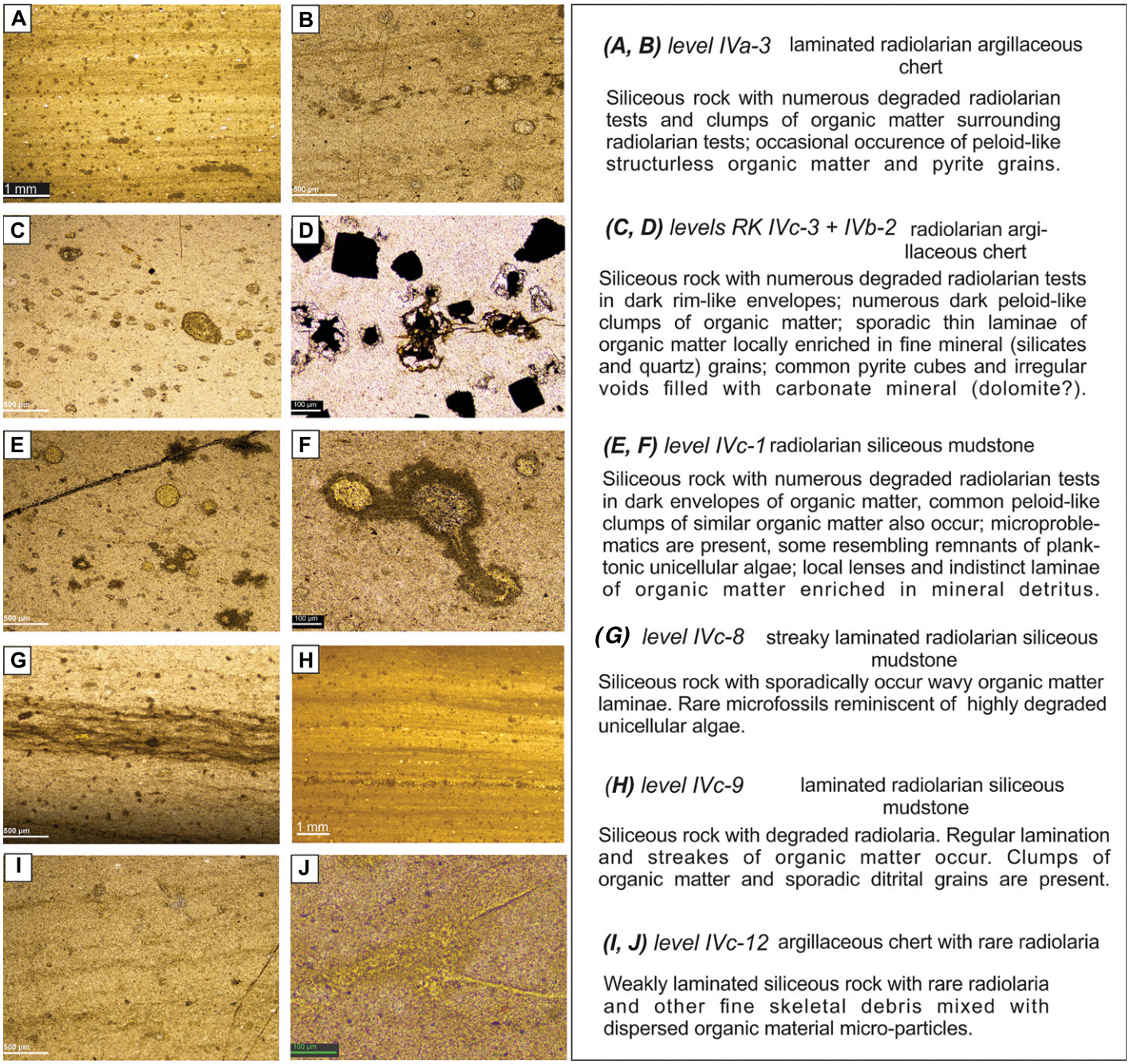

Figure 9. Stratigraphic variation of Famennian chert microfacies in the composite Bardo IV section (for sample locations and petrographic categories see Figs. 2A and 11).

implications. However, this is undoubtedly true for rhythmic chert/shaly successions, in which silica migrated from the host clayey lithologies toward cherty precursors. In the case of an overall uniform lithological setting, such as in the Bardo succession, the inter-bed diagenetic transfer seems less probable. This supposition is confirmed by a distinctive four-step secular chemostratigraphical pattern, related to primary depositional characters (see below). Also, a significant correlation of biogenic Si and P ($r_s = 0.61$) is a valid test because they are key elements showing opposite diagenetic tendencies during the formation of cherts: a major addition of Si and depletion of P (Murray, 1994). This is the rationale for further chemostratigraphic study.

The studied cherts show a good positive correlation between Al_2O_3 and $\Sigma REE + Y$ ($r_s = 0.84$), and an REE pattern similar to that of upper continental crust, given that the elements are largely derived from terrigenous sources. The excess $\Sigma REE + Y$ contents caused by adsorption from seawater in open-ocean basins are higher than those near the continental margin (Murray et al., 1992). The cherts have average Ce/Ce* (1.08 ± 0.06) and Y/Ho (26 ± 1.85) values characteristic for rocks deposited in a continental margin setting. Furthermore, low values of the Mn/Ti ratio (below

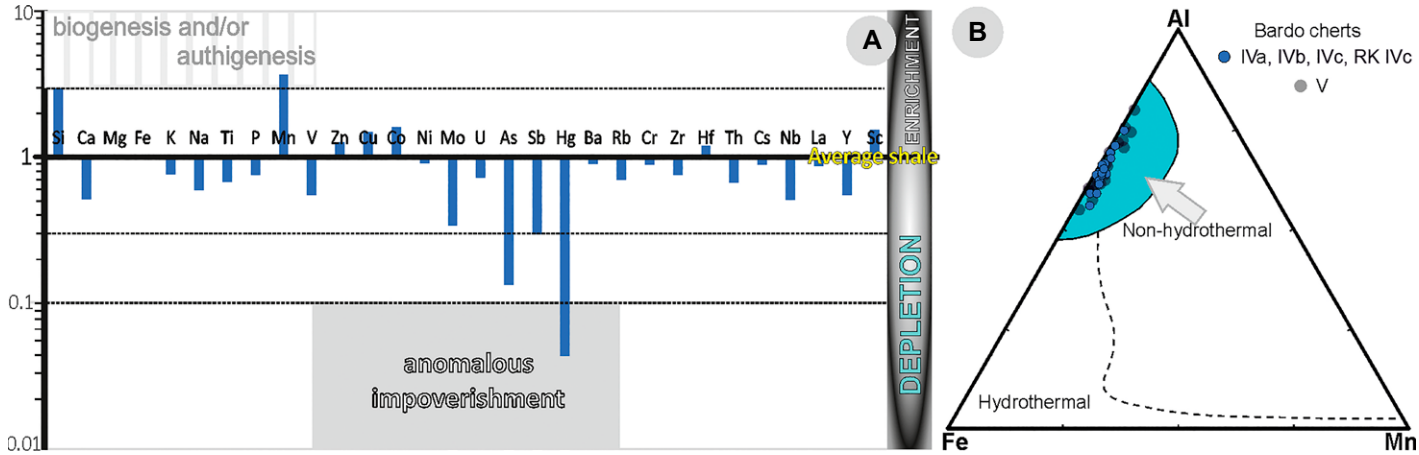

Figure 10. (A) Enrichment/depletion patterns of selected elements from the Famennian siliceous-clayey rocks at Bardo IV, in SW Poland, against the average shale of Wedepohl (1971; see Table 2). Three- and ten-fold values of enrichment/depletion ratios are used as thresholds (see Racki, 2020). (B) Al-Fe-Mn diagram showing samples from the Bardo radiolarian cherts only in the non-hydrothermal (hydrogenous) field. Hydrothermal and non-hydrothermal fields are after Adachi et al. (1986, their fig. 5), modified by Liao et al. (2019, their fig. 5).

0.5; Udchachon et al., 2017) also suggest the most nearshore deposition in the lowest interval (Figs. 12 and Fig. 13B).

Weathering and Climatic Setting in Sediment Source Areas

Because rapid climate changes are well known from the terminal Devonian time, culminated in a short-lived glaciation after a transient greenhouse Hangenberg Crisis episode (see summaries of Kaiser et al., 2016 and Aretz, 2020), select climate proxies were tested in the Bardo succession. The seventeen proxies analyzed (see Supplemental Material S3) are sensitive to the behavior of elements in two climate extremes: humid/greenhouse and arid/icehouse, and therefore they record weathering conditions in source areas of the clastic contamination in the chert, in particular intensive rainfalls and chemical weathering under hot and moist conditions (Ratcliffe et al., 2010; Rothwell and Croudace, 2015; Ferriday and Montenari, 2016; Lash, 2017; Lo et al., 2017; Craigie, 2018; Racki et al., 2019; Prajith et al., 2021).

Considering the proxies at the Bardo IV section, most of the estimates exhibit the same major secular trend toward the end-Devonian icehouse (Kaiser et al., 2016), exemplified by Ga/Rb ratios (Fig. 12), but in detail obscured by their irregularly oscillating values. The tracer especially positively links with nine proxies ($r_s > 0.62$), such as Th/K, K/Al, and Rb/Al. The estimates indicate greenhouse pulses of elevated weathering rate, mostly corresponding to increased detrital input, in particular in the II–IV interval, as well as cooling intervals paired with increased biosiliceous productivity.

Hydrothermal Activity, Redox Conditions, and Bioproductivity

Chalco- and siderophile constituents are not characterized by enrichments in the Bardo clayey cherts (Table 1; Fig. 10A), but a coherent group, including such elements as Mo, Cu, Zn, Pb, U, and As as well as Co, Ni, V, and Sb in part (see Supplemental Material S3) reveals significant mutual associations ($r_s > 0.5$). The elements are notably independent in distribution from the aluminosilicate phase. Thus, they may be considered an authigenic biogenic-dominated constituent (Tribovillard et al., 2006; Algeo and Liu, 2020; Bennett and Canfield, 2020). However, the constituents may be also affected by differential fluid delivery from the sea-floor vents (Grenne and Slack, 2005; German and Von Damm, 2006; Fig. 12), and by eruptive gaseous emissions (Oppenheimer, 2014; Yudovich and Ketris, 2015). Several geochemical proxies, such as moderate iron and manganese values ($Fe_2O_3 < 5.3\%$, $MnO_2 < 0.4\%$; Fig. 10; Table 2), relatively high values of the Al/(Al + Fe + Mn) ratio (>0.6; Fig. 12), and low Hg contents (median 30.7 ppb; Fig. 10A) suggest that the cherts largely originated from marine water without significant hydrothermal and volcanic inputs (Murray et al., 1992; Grasby et al., 2019; Jones et al., 2019; Hou et al., 2021).

The very low TOC contents, mostly ~0.1%, characterize the studied cherts, and the post-depositional processes, especially weathering, could bias all OM and pyrite hosted trace metals (Derkowski and Marynowski, 2018). However, this impoverishment characterized some black Paleozoic radiolarian cherts (table 4 in Cressman, 1962), as well as dark cherty strata from the D-C transition in southeastern China (Shijia section; Racki, 2020, Supplemental Material 3 therein) and Bavarian cherts (Table 2). Oceanic siliceous sediments are overall depleted in OM due to degradation within the water column (tables 18 and 22 in Ronov et al., 1991). The first-order trend is certainly preserved, as reflected in the organic-enriched Bardo IVa samples (TOC content 0.5%–1.3%; see below). Thus, oligotrophic regimes and low primary production levels are thought to have dominated in the middle Famennian basin.

A tendency toward some basin restriction, of the Black Sea type, is suggested by the composite proxy of Cd/Mo versus Co × Mn (Fig. 13A), that was proposed—on the actualistic basis—by Sweere et al. (2016; see also Yang et al., 2021). On the other hand, analogies with the Arabian Sea are remarkably recorded in the end-Famennian interval. The sea shows only seasonal upwelling and a less distinct oxygen minimum zone (OMZ), and therefore its sediments have lowered OM contents. Furthermore, a similar conclusion derives from distribution of Mo (<23 ppm), V (<5 ppm), and U (>1 ppm) enrichments, i.e., diagnostic of oxic regimes "beneath the core of a perennial OMZ environment" (Bennett and Canfield, 2020). Accordingly, it is likely that the more advanced anoxia only transiently developed in the Bardo Basin.

Provenance and Tectonic Setting

The clear differentiation of depositional and igneous signatures (see Supplemental Material S3) indicates that the contemporaneous eruptive activity only episodically contributed direct input to the oceanic basin (see below). However,

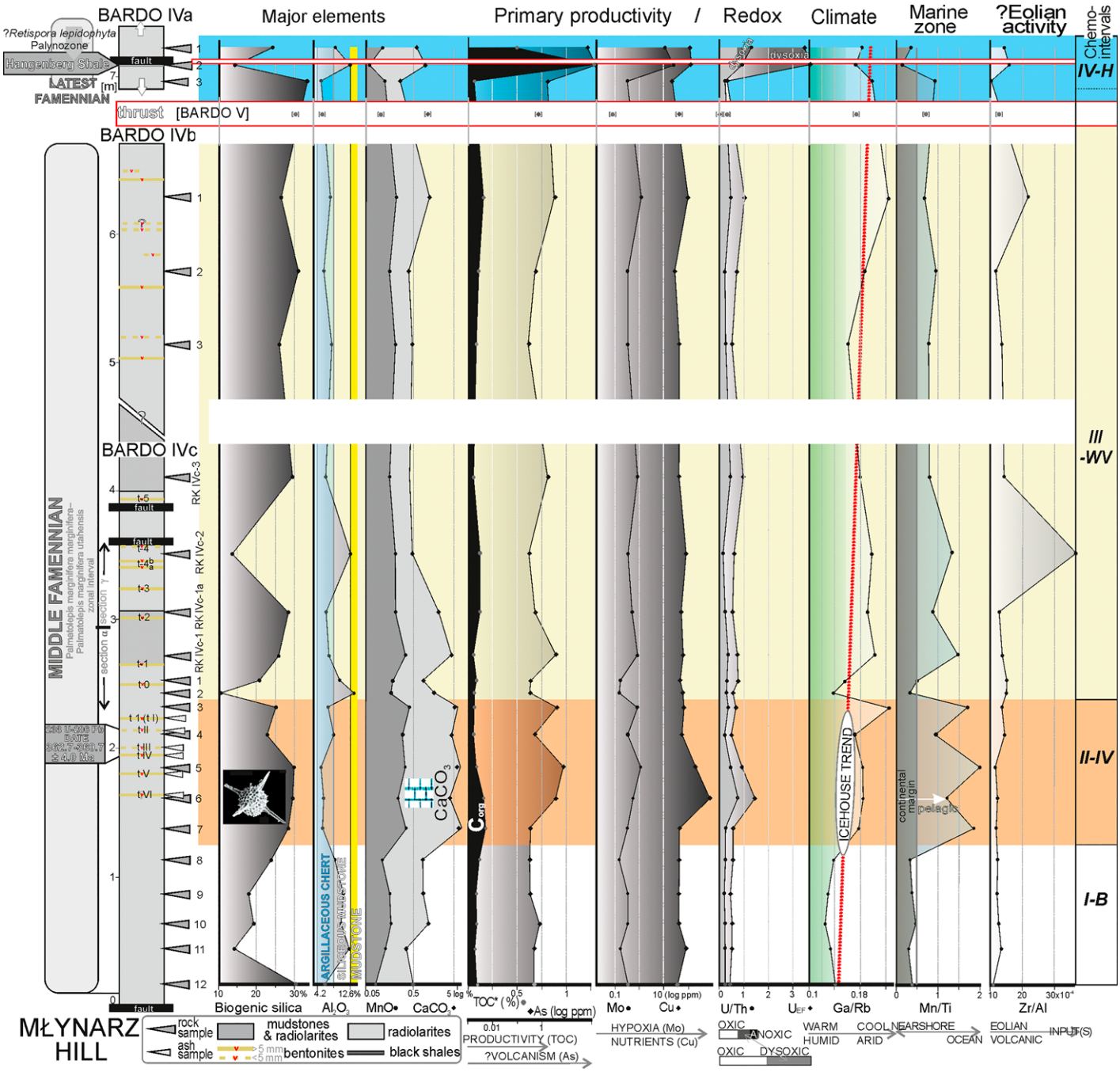

Figure 11. Stratigraphical trends of selected geochemical proxies for major elements, bioproductivity/redox states, climate, and paleogeography in the composite siliceous-clayey Bardo IV succession of SW Poland (see Figs. 2A and 8). Note information gaps corresponding to tectonic contacts and extended sampling intervals, as well as fragmentary IVa succession limited to the sampled interval. The maximum $CaCO_3$ contents are estimated approximately from the CaO concentrations; correlative links between Ca and Mn, due to presence of Mn-enriched calcite (M. Szczerba, email communication, 2020), are notably. Petrographic categories of siliceous-clayey rocks after Jones and Murchey (1986, their fig. 1). The medians of 22 samples from the supplementary topmost Famennian Bardo V section (Fig. 1B), thought as environmental complementation in the tectonic gap in the Bardo IV succession (Fig. 8), are added. Note the logarithmic scale for As, Mo, and Cu. TOC—total organic carbon.

the various provenance proxies proposed in the literature give somewhat ambiguous results (see their critical review in Armstrong-Altrin and Verma, 2005).

Weathered and eroded substrates were generally similar in composition to the average upper continental crust (i.e., andesite-like), as exemplified by Cr/Nb and Th/Sc time series (Fig. 12; see Cullers, 2000; Środoń et al., 2014). The same affinity with average shale standards is shown by Th/Sc versus Zr/Sc (McLennan et al., 1993), and relationships between K_2O

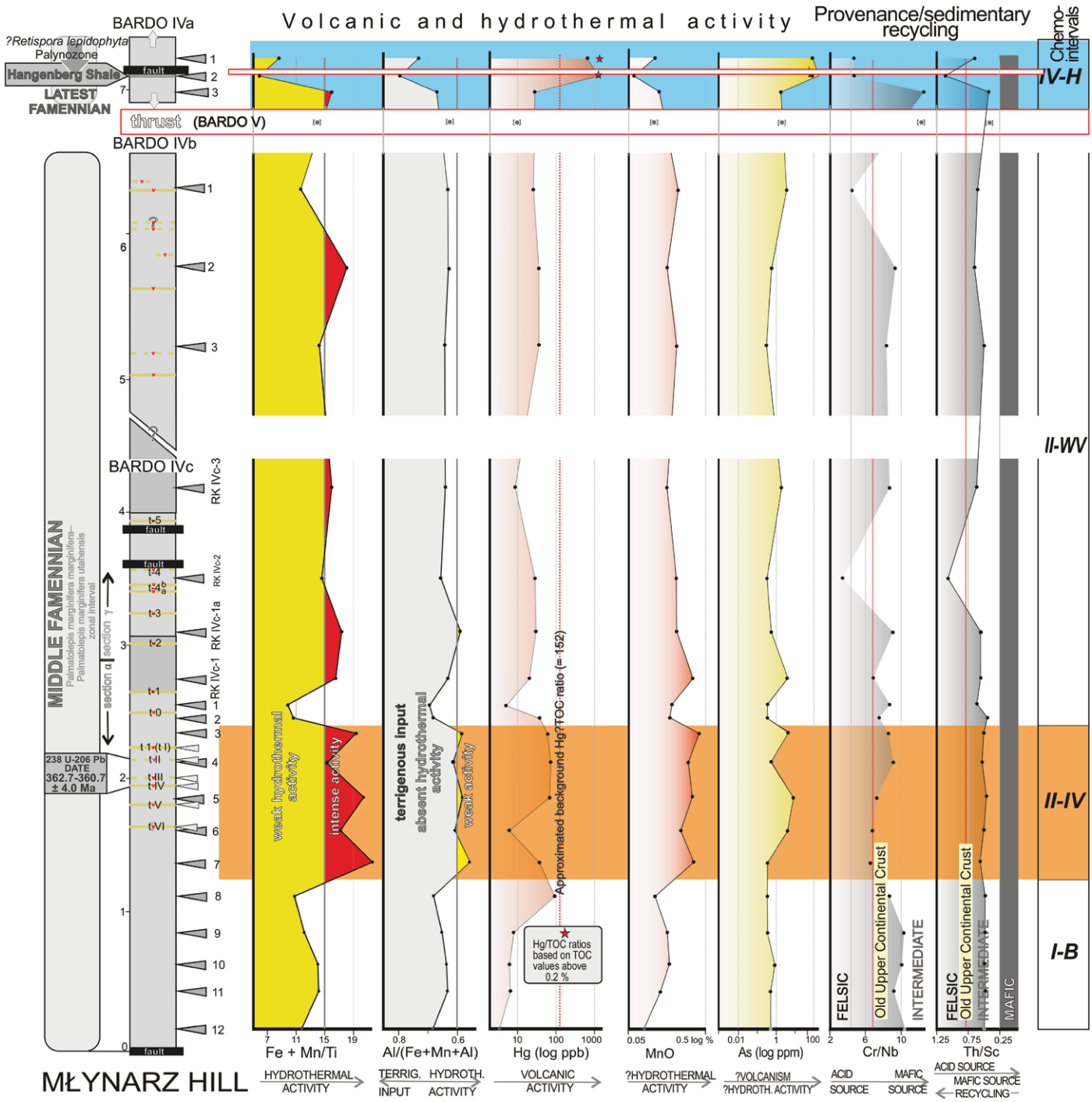

Figure 12. Stratigraphical trends of selected geochemical proxies for volcanic and hydrothermal activity, and provenance/recycling in the composite siliceous-clayey Bardo IV succession from SW Poland (see explanations in Fig. 11). Note that only two values of Hg/TOC ratio are marked (asterisked) because of their mostly very low total organic carbon (TOC) contents (<0.2%), and a background Hg/TOC level which is approximated for the sample set following Racki (2020). Thresholds for hydrothermal processes after Böstrom (1983) and Wang et al. (2020), for Cr/Nb and Th/Sc ratios indicating sources of terrigenous fraction after Cullers (2000, their table 3, compare Fig. S4/2 and Table 3) and Rudnick and Gao (2003). Note reversed scale for the Al-based hydrothermal proxy and logarithmic scales for generally impoverished Hg and As (see Fig. 10A).

and Rb, La/Th versus Hf, and Th/Ni versus Zr/Ni (adopted from Ran et al., 2015; Francovschi et al., 2020, and references therein). The application of Th, Sc, Cr, and La ratios as provenance indicators (La/Sc, Th/Sc, Th/Cr, and Eu/Eu* normalized to chondrite) confirm a source with a felsic to intermediate composition (see Table 3). Small positive Ce anomalies and a negligible LREE depletion with respect to

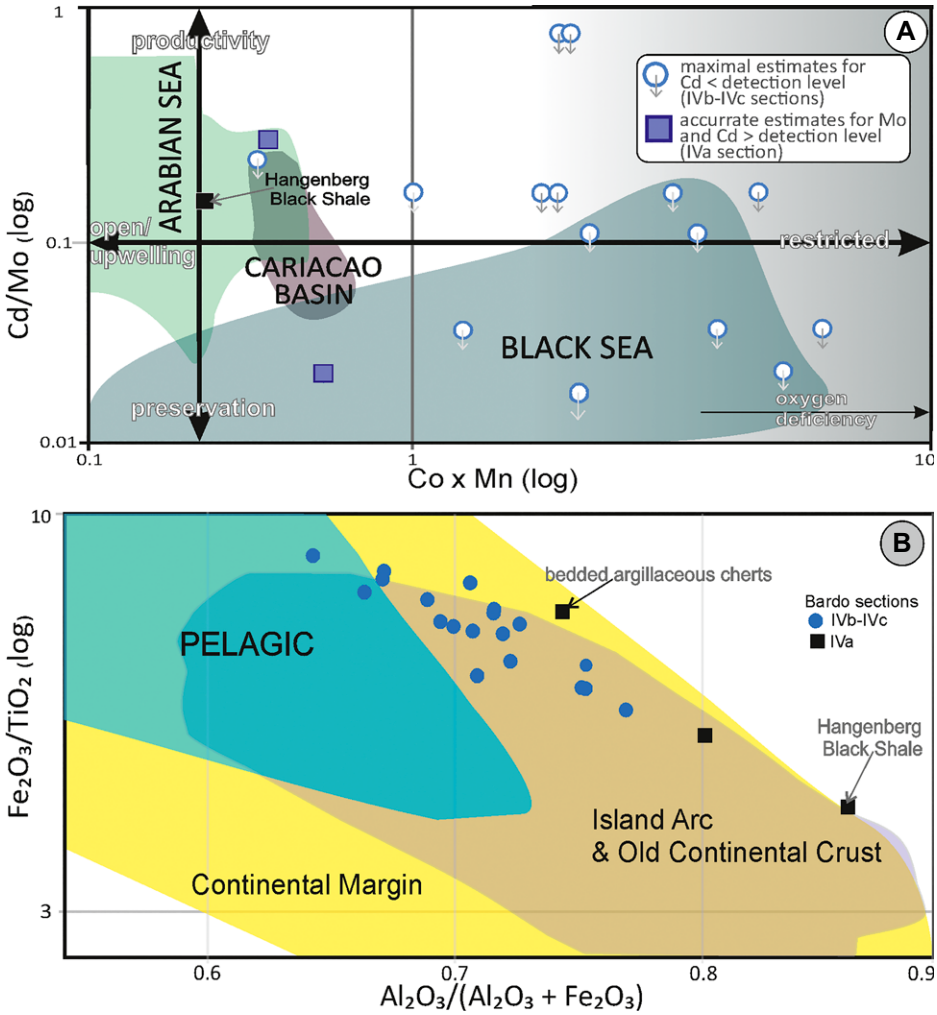

Figure 13. Discrimination diagrams illustrating environmental setting of the cherty rocks from the Bardo IV locality in SW Poland; note distinctly specific position the Hangenberg Black Shale. (A) Environmental distinction based on Cd/Mo and Co × Mn proxies (adopted fig. 7 from Sweere et al., 2016). Note mostly approximate Cd/Mo ratios of samples IVb and IVc due to the Cd depletion. (B) Diagram of Fe_2O_3/TiO_2 and $Al_2O_3/(Al_2O_3 + Fe_2O_3)$, showing the ratios plot of the Bardo cherts at the continental margin field, and only two samples possibly at the pelagic area (based on fig. 16 of Ran et al., 2015; Zong et al., 2016, their fig. 6); the fields are from Murray (1994).

HREE for the samples from the Bardo sections point to an origin within a continental margin setting (Fig. S4/1). However, in the Fe_2O_3/TiO_2 versus $Al_2O_3/(Al_2O_3 + Fe_2O_3)$ and La_N/Ce_N versus $Al_2O_3/(Al_2O_3 + Fe_2O_3)$ discrimination diagrams, the studied chert samples plot almost entirely in the subfields defined by sediment derived from old upper continental crust and rocks from the basalt-andesite series of island arcs (Figs. 13B and 14A, see also the La-Th-Sc and (Th-Sc-Zr)/10 diagrams in Fig. S4/2). In brief, most of the tracers suggest andesitic to granodioritic debris composition shed from proximal continental-island arc areas. Thus, Cadomian orogenic crust could be a source for the Famennian allochthon sediments of the Bardo Unit, as proposed by Mazur et al. (2015).

FAMENNIAN VOLCANIC ACTIVITY

Intercalations of white kaolinite-rich shales were noted in siliceous Brzeźnica beds by Oberc (1957, p. 30), but never considered as a volcanic signature. At least 15 pale-yellow volcaniclastic intercalations are recognized in the Brzeźnica beds in the Bardo IVc section (Figs. 2 and 4B), and the igneous activity can be presumed for the middle Famennian (Fig. 8).

Several trace elements are considered to be immobile during diagenetic alteration and reliable proxies of petrogenetic processes (Huff, 2016; Pointon et al., 2018). Whole-rock geochemical data from six tephra samples point to their Al-bentonite assignment (see K_2O versus Al_2O diagram of Kiipli, 2021; Fig. 15A), that characterized the likely initial stage of this Variscan volcanism. In terms of tectonic environment, the Al bentonites are suggestive of a convergent margin origin (Figs. 15B–15D; Fig. S4/3) and correlate well with Devonian metavolcanites of the Western Volcanic Belt (Janoušek et al., 2014) and some ashes of the Variscan belt, including pre-Hangenberg volcaniclastics from the Holy Cross Mountains. (Pisarzowska et al., 2020). Interestingly, the late Viséan bentonites from the autochthonous section of the Bardo Unit (Paprotnia Beds) also record explosive andesite-rhyolitic magmatic sources from a continental margin setting (Kryza et al., 2011).

OCEANIC RECORD OF THE HANGENBERG BLACK SHALE

The black slate horizon (IVa/2) in the highest part of the Bardo IV cherty succession represents a unique lithology (Fig. 3B) that is clearly distinct from the organic-poor siliceous-clayey depositional background of the section (Figs. 11–13; Table 3). Its distinguishing features include:

- Mo- and U-based proxies indicating a hypoxic oceanic event.
- Flourishing primary production indicated by high OM content (TOC = 1.3%). High Cu and P/Al values as well as Zn and Pb spikes suggest an increase in eutrophication.
- The transient turnover of bioproductivity which corresponds to the growing detrital supply observed not only in the slightly increased clay content, but also in the mixed marine-terrestrial palynofacies (Fig. 6). Increased aeolian activity is therefore suggested by the increased supply of mud-class quartz fraction with higher Zr/Al and Zr × Hf /Al ratios (Calvert and Pedersen, 2007). However, in the middle Famennian interval III WV, at least two episodes of more intense atmospheric dust transport and/or pyroclastic addition were recognized.
- As for the provenance, the shale consistently reveals the most continental "old" felsic sources (from an uplifted block?), as exemplified by Th/Sc ratios and Cr/Nb ratios (Fig. 12; Table 3). This conclusion is supported by Hf versus La/Th (Fig. 14B), as well as La/Sc, Th/Cr, and Eu/Eu* ratios.
- This end-Famennian interval was marked by a fluctuating climatic setting (Kaiser et al., 2016), more or less confirmed by several

TABLE 2. MEDIAN CONCENTRATIONS OF SELECTED ELEMENTS IN THE BARDO IV SECTION UNDER STUDY, SW POLAND

Element	Average shale (Wedepohl, 1970, 1971)	Post-Archean Australian shale (PAAS) (Taylor and McLennan, 1985)	Saxo-thuringian Famennian shale (Romer and Hahne, 2010)	Average cherty shale (Ketris and Yudovich, 2009, major elements after Ronov et al., 1991†)	Average siliceous mudstone (Barrett, 1981§)	Upper continental crust (Rudnick and Gao, 2003)	Famennian radiolarian cherts of Bavaria# (median)	Bardo radiolarian cherts (median)
Major elements (%)								
Al	8.9	10.0	12.0	*2.4*	4.1	8.16	2.7	**4.0**
Si	27.7	29.4	24.3	*38.5*	38.9	31.3	39.2	**38.0**
Ca	1.6	0.93	0.5	*1.02*	0.06	2.55	0.05	**0.37**
Mg	1.6	1.33	1.41	*0.56*	0.71	1.49	0.46	**0.75**
Fe	4.8	5.05	6.76	*1.79*	2.68	3.92	1.62	**2.11**
K	3.0	3.07	3.65	*0.91*	1.44	2.32	0.90	**1.03**
Na	1.2	0.89	0.47	*0.33*	0.05	2.42	0.46	**0.32**
C_{org}	0.7*	x	0.54	*0.5*	x	x	0.1	**0.1**
Minor and trace elements (ppm)								
Ti	4600	6000	9440	2100 (*1680*)	1740	3840	1350	**1400**
P	704	700	*785*	1200 (*675*)	352	660	242	**240**
Mn	850	900	1517	250 (*2325*)	1006	774	1890	**1400**
V	130	150	148	250	x	97	35	**32**
Zn	95	85	114	160	74	67	24	**52.5**
Pb	22	20	4.2	12	6	11	2	**11.7**
Cu	45	50	x	100	35	28	40	**30.2**
Co	19	23	23	11	30	17.3	8	**13.7**
Ni	68	55	64	63	72	47	20	**27.7**
Mo	1.3	1	0.3	29	x	1.1	0.4	**0.2**
Cd	0.13	x	x	9	x	0.1	<0.1	**<0.1**
U	3.7	3.1	2.2	13	x	2.7	0.7	**1.2**
As	10	x	x	30	x	4.8	2	**0.6**
Sb	1.5	x	0.7	8.8	x	0.4	<0.1	**0.2**
Hg	0.4	x	x	0.18	x	0.05	<0.01	**0.03****
Ba	580	650	1010	740	140	628	131	**236**
Rb	140	160	156	47	88	112	42	**44.2**
Cr	90	110	106	86	31	92	46	**36**
Zr	160	210	234	140	61	193	41	**54.4**
Hf	2,8	5	x	3.1	x	5.3	1.2	**1.5**
Th	12	14.6	13.2	4.2	x	10.5	3.2	**3.6**
Cs	5.5	15	6.5	3	x	4.9	1.7	**2.2**
Nb	18	19	x	17	6	12	4.6	**4.4**
La	40	38	41	31	x	31	13	**15.7**
Y	41	27	x	25	15	21	10.2	**10.1**
Sc	13	16	20	12	x	14	6	**9**
Ga	19	20	30	14	x	17.5	5.3	**7.7**

Notes: Against three average shales, coeval Saxothuringian shale and cherts, and upper continental crust abundance levels (x—not determined); above three-fold depletion against average cherty shale for minor and trace elements in light gray, and anomalous depletion above ten-fold values in dark gray, and above three-fold enrichment in yellow (Fig. 10A). C_{org}—organic carbon; *C_{org} is calculated from data in Wedepohl (1970).

†The major element values (*italicized*) refer to siliceous rock of "continental geosynclines" (table 15 in Ronov et al., 1991).

§Upper mudstone bed in tables 1 and 2 in Barrett (1981).

#Based on five samples of radiolarian cherts from the Rauheberg locality in the Frankenwald (northern Bavaria, Kiessling and Tragelehn, 1994; Supplemental Material S3).

**According to atomic absorption spectrometry data (but <0.01 ppm in inductively coupled plasma–mass spectrometry results).

proxies, e.g., Th/Rb, Al/Ti, Sr/Ba, and Mg/Al ratios.

- Intense eruptive activity can be inferred from the coupled anomalous Hg enrichments and higher Hg/TOC ratios (see discussion in Pisarzowska et al., 2020 and Racki, 2020), as well as from the enrichment factor of Cs spike and high As concentrations (Ratcliffe et al., 2010; Racki et al., 2019). Occurrence of miospore tetrads (Fig. 6: see nos. 9 and 10) confirm extreme high-stress conditions, possibly even ultraviolet driven mutagenesis (Filipiak and Racki, 2010; Marshall et al., 2020).

Considering all these features as well as the age constraints, we can correlate the shale intercalation in the topmost Bardo IV section to the worldwide Hangenberg Black Shale (HBS, Fig. 16), they key event in a multi-stage global change (see Pisarzowska et al., 2020; Racki, 2020; Aretz et al., 2021).

Notably, two contrasting types of the D-C passage beds are documented in the Bardo Unit, considered to be the easternmost part of the waning Saxothuringian Ocean (Figs. 17 and 18). First, the carbonate-dominated section in the inner Bardo Ocean (Wapnica, Gołogłowy; Haydukiewicz, 1979; Matyja et al., 2021; see also the Zdanów 1 borehole section in Chorowska et al., 1992), and second, the cherty succession in the outer basin (Fig. 18C). In light of biostratigraphical data of Matyja et al. (2021; Fig. 6: see nos. 22–25), the occurrence of the HBS is assumed in both domains. Thus, as shown above, the main environmental disruption took place in the Sudetic domain just ahead of the D-C boundary during this global anoxic event. In addition, a difference in provenance is recognized between the autochthonous and allochthonous successions, i.e., intermediate to felsic source for the Bardo site, and intermediate to mafic source for the Wapnica section (Fig. 14B). This is a plausible corollary considering that the Wapnica

TABLE 3. THE PROVENANCE RATIOS (CULLERS, 2000) CALCULATED FOR THE FAMENNIAN CHERT, BENTONITE, AND SHALE SAMPLES FROM THE BARDO IV LOCALITY, SW POLAND

Proxy	UCC	PAAS	Range of sediment from felsic sources fine fraction	Range of sediment from mafic sources fine fraction	Chert (n = 21)	Bentonite (n = 6)	HB Black shale (n = 1)
La/Sc	2.21	2.39	0.7–27.7	0.4–1.1	1.47–3.23 (avr. 2.03)	0.66–3.79 (avr. 1.42)	3.03
Th/Sc	0.79	0.91	0.64–18.1	0.05–0.4	0.43–1.07 (avr. 0.55)	0.67–1.08 (avr. 0.87)	1.11
Th/Cr	0.13	0.13	0.067–4.0	0.002–0.045	0.05–0.26 (avr. 0.11)	0.36–0.91 (avr. 0.67)	0.2
Eu/Eu*	0.65	0.65	0.32–0.83	0.7–1.02	0.58–0.88 (avr. 0.72)	0.63–0.73 (avr. 0.67)	0.64

Note: Eu/Eu*—chondrite-normalized after McLennan (2001); UCC—upper continental crust; PAAS—Post Archean Australian Shale; HB—Hangenberg; avr.—average.

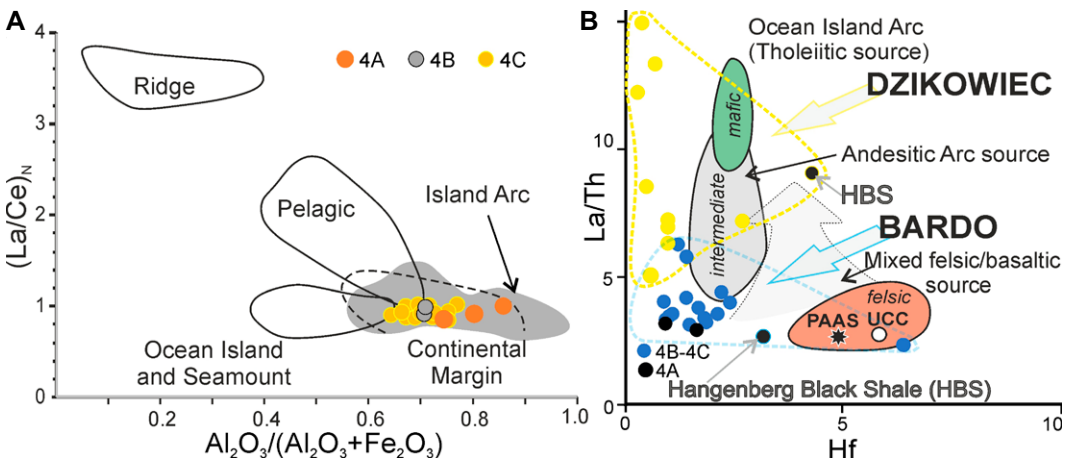

Figure 14. (A) $(La/Ce)_n$ versus $Al_2O_3/(Al_2O_3 + Fe_2O_3)$ discrimination diagram for the Bardo IV and V chert samples of SW Poland. The fields labeled Ridge, Pelagic, and Continental Margin are from Murray (1994); the Island Arc field is after Girty et al. (1996). (B) Comparison of the Bardo (allochthonous) and Dzikowiec (autochthonous) Devonian-Carboniferous successions, in SW Poland, in terms of provenance (after Floyd and Leveridge, 1987). PAAS—Post-Archean Australian Shale; UCC—upper continental crust (see Table 2).

succession onlaps the Nowa Ruda gabbroic massif that belongs to the Central Sudetic Ophiolite.

EVENT CHEMOSTRATIGRAPHY AND ENVIRONMENTAL EVOLUTION

Considering geochemical time series and other multiproxy data in the interrupted middle and latest Famennian framework (Figs. 11 and 12), four intervals are distinguished in the Bardo IV section (Fig. 16). The subdivision of this succession is not based on rapid temporal changes to key elements and is therefore not defined in terms of chemozones (*sensu* Craigie, 2018), but rather the subdivision corresponds to developmental stages of the basin.

Because volcanic ashes were not recorded in other Famennian sections of the Bardo Mountains (Oberc, 1957; Haydukiewicz, 1979; Cymerman et al., 2015), their lowest occurrence in the Bardo IV locality is therefore seen as onset of regional volcanic activity. The middle Famennian explosive outburst and intensified hydrothermal processes were determined in the transgressive and likely highly productive basin during the II-IW interval (Fig. 11). The activity gradually waned in the III-WV slice, while a well-known paroxysm revived in the Hangenberg crisis time (Menor-Salván et al., 2010; Pisarzowska et al., 2020; Racki, 2020).

Geochemical data for the Bardo V section correspond well with the upper III WV interval, complementing the facies evolution recognized in the tectonized Bardo IV succession (Figs. 8, 10B, 11, and 12; Figs. S4/1–2). The HBS is absent in the site, likely due to a tectonic gap. Only single horizons indicate either a more oxygen-depleted regime or an increased volcanic ash delivery in the latest Famennian. Thus, an overall monotonous biosiliceous-clayey deposition is assumed throughout the middle-latest Famennian in the Bardo Basin.

DISCUSSION

Several controversial aspects of the paleogeographic affinities with the Bavarian segment of the Saxothuringian Zone may be partly verified (Fig. 17), in association with the Variscan volcanic activity in front of the NE shelf of Gondwana (Kryza et al., 2004; Mazur et al., 2006, 2015; Franke et al., 2017; Golonka, 2020). Toward a more precise definition of the composite Bardo Ocean (Wajsprych, 1986, 1995, 2008), the term "outer Bardo Ocean" is applied here to the parental "lost" pelagic sedimentary basin, as fragmentarily preserved by the allochthonous Bardo series, versus the "inner Bardo Ocean" recorded in the autochthonous succession.

Siliceous Facies of the Bardo Basin

The multiproxy data comprehensively document the evolving deep-water deposition in the outer Bardo Ocean (Fig. 18), which has distinctive oceanic attributes comparable to other fluctuating but mostly oligotrophic regimes with low primary production levels, influenced by weak upwellings below the perennial oxygen minimum zone. The factors controlled by interplay between biosiliceous and—generally declining—siliciclastic deposition. Episodic eutrophication and recurrent radiolarian blooms, thought to be tied to orbital cycling (De Wever et al., 2001, p. 67), were likely also associated with the circulation of nutrient-rich cold currents, as assumed for the Kulm facies (Randon and Caridroit, 2008). The basin was at least 1 km deep, in line with the hypothesis of the carbonate compensation depth at that time (Racki and Cordey, 2000, their fig. 3), conodont palmatolepid biofacies (Table 1; Haydukiewicz, 1998, 2002), and supposed graptoloids (Fig. 2D), and microfacies characters (Fig. 9). The first-order control included regional tectonic and volcanic activity, superimposed on the global climatic and oceanographic trends (Menor-Salván et al., 2010; Kaiser et al., 2016; Aretz, 2020). The factors controlled the evolving dynamics between fine clastic delivery via wind, and perhaps by diluted tempestite/turbidite currents (Fig. 2B), and biosiliceous production, limited by the available Si nutrient reservoir (Racki and Cordey, 2000; De Wever et al., 2001, p. 46–54; Hüneke and Henrich, 2011; Cecil, 2015; Lazarus et al., 2020, p. 217–225). Similar hemipelagic deposition can be assumed for other Famennian siliceous successions in the Saxothuringian Zone, based on geochemical data from Bavarian cherts (Table 2), as well as similar coeval cherty strata in China (Zhang et al., 2020). However, very poor preservation of opaline tests suggest fluctuations in silica saturation in the water column in the outer Bardo Ocean (see De Wever et al., 2001, p. 37–39; Lazarus et al., 2020, p. 218–222), unlike the Bavarian Ocean (see fig. 3 in Kiessling and Tragelehn, 1994).

In the context of the changing middle Paleozoic marine conditions in the Central Sudetic domain, macro-morphological and lithological similarity of the Famennian cherts to the early Silurian radiolarites from the Bardo Mountains does not imply a similar depositional environment for these rocks. In particular, lamination in the Silurian cherts, expressed by the presence of benthic microbial mats, is common, well-developed and regular, while only fine hemipelagic lamination is recognizable in the Devonian oceanic rocks (Figs. 9A and 9H; compare e.g., siliceous turbidites of Nisbet and Price,

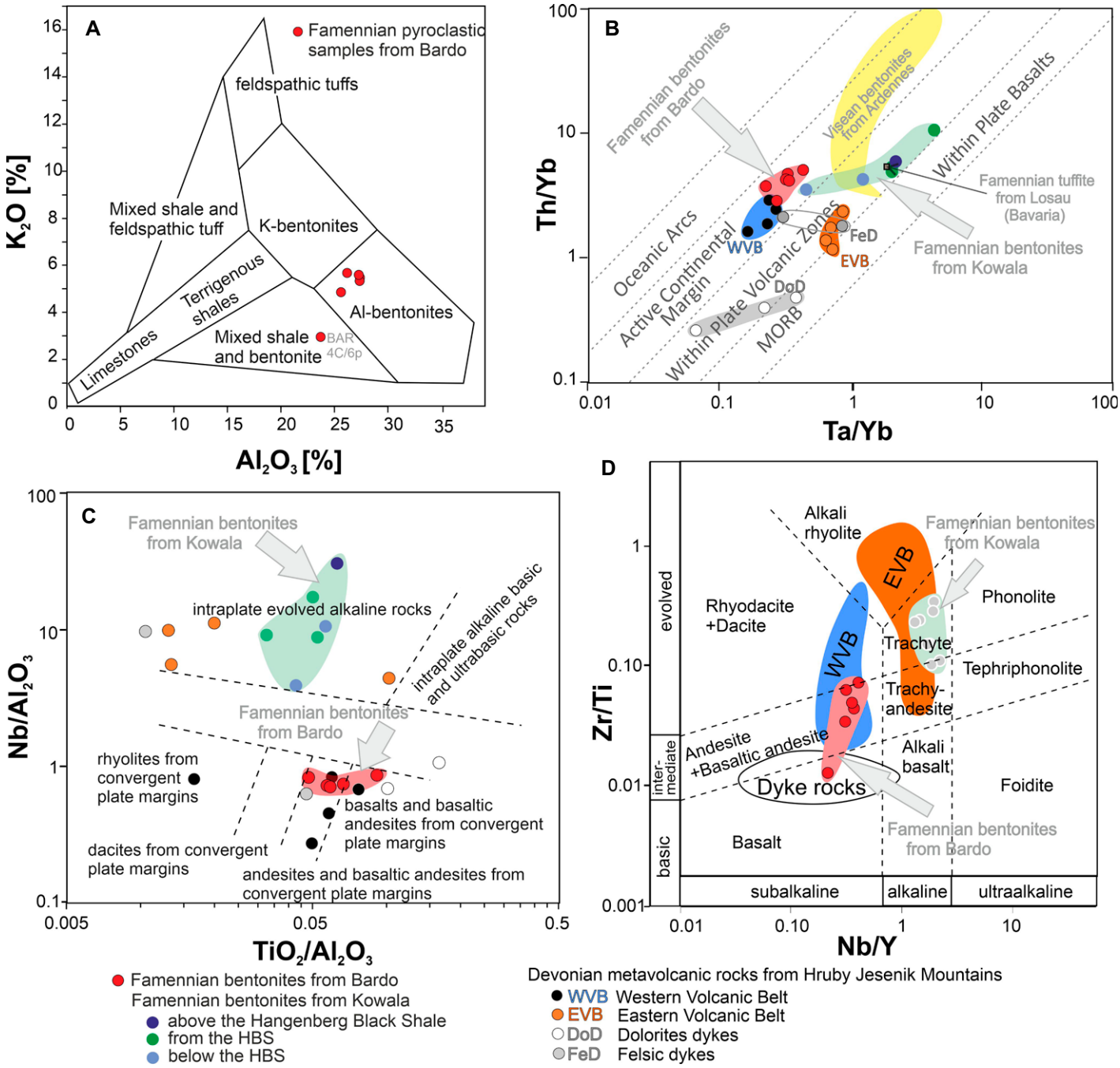

Figure 15. (A) Al_2O_3-K_2O chart (after Kiipli, 2021) and trace elements (B–D) distribution diagrams of the Famennian bentonite samples from Bardo IVc and other Devonian-Carboniferous successions of SW Poland. TiO_2/Al_2O_3[%] versus Nb[ppm]/Al_2O_3[%] chart of Kiipli et al. (2020). Nb/Y versus Zr/Ti diagram of Winchester and Floyd (1977) modified by Pearce (1996), showing Bardo ashes mainly in andesite and basaltic andesite field. The metavolcanic rocks from the Vrbno Group, Bohemian Massif (WVB—Western Volcanic Belt; EVB—Eastern Volcanic Belt). End-Famennian and Viséan pyroclastic data from the Holy Cross Mountains (Kowala, Kielce County, Central Poland, Pisarzowska et al., 2020), Bavaria (Losau, Germany, Racki, 2020), Ardennes, Belgium (Pointon et al., 2018), and Bohemian Massif (Hrubý Jeseník Mountains, Czech Republic; Janoušek et al., 2014) shown for comparison. MORB—mid-ocean ridge basalt; HBS—Hangenberg Black Shale.

1974). The Silurian and Devonian cherts differ also in silica content. In the early Silurian pure radiolarites, the content of silica is significant, exceeding 95% SiO_2. Devonian cherts contain 70 to 90% SiO_2. In fact, Silurian black cherts are products of shallow to moderately deep epicontinental seas, within the photic zone up to 400 m, but probably much shallower (Kremer and Kaźmierczak, 2005; Kremer, 2020). Silurian radiolarites are composed predominantly of remains of radiolarian and well-preserved cyanobacterial mats, even at the level of individual

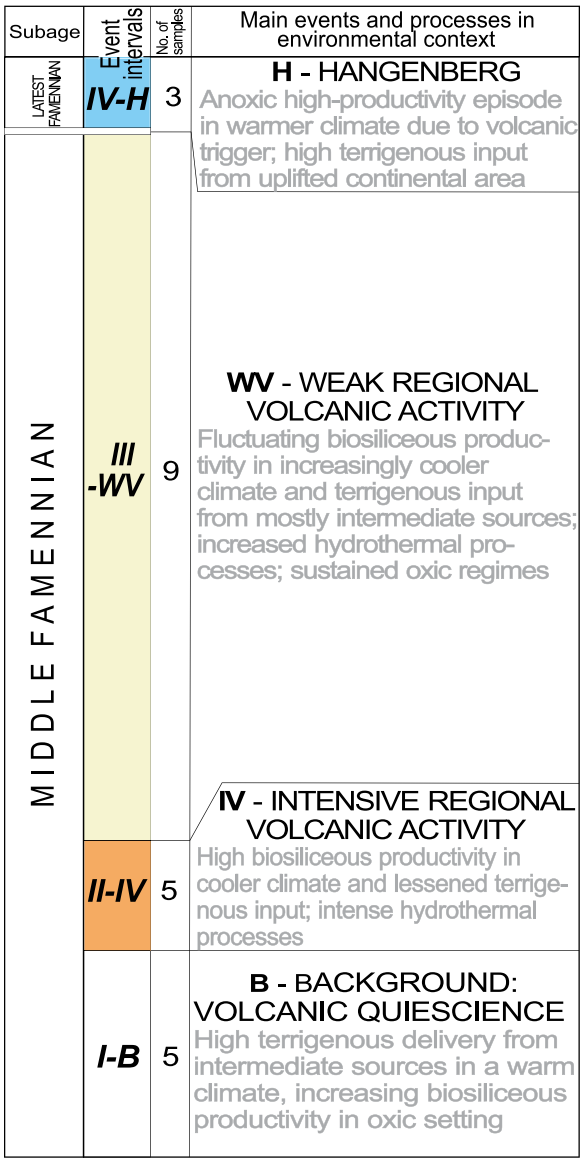

Figure 16. Event chemostratigraphy scheme for the Bardo outer ocean, summarizing the geochemical data for the Bardo IV succession of SW Poland (see Figs. 12–14).

coccoid cells. Particularly frequent are acritarchs and other unicellular algae, including ones that inhabited the water column. The microbial community indicates high primary productivity of the early Silurian sea compared to the Famennian ocean.

Toward a Tectonic Model

The Bardo Basin was initiated in the late Frasnian, not later than 10 m.y. after the emplacement of the Central Sudetic nappes and cessation of regional metamorphism (post-early Givetian; Hladil et al., 1999). The basin partly onlaps the Góry Sowie Massif (Chorowska et al., 1992), the most prominent Central Sudetic nappe (Mazur et al., 2006), that had been exhumed from mantle depths starting from the Early Devonian (O'Brien et al., 1997; Tabaud et al., 2021). Continental subduction of the Góry Sowie Massif was related to the consumption of an unknown early Paleozoic oceanic domain. This process was coeval with the opening of the Devonian short-lived Central Sudetic Ocean (Awdankiewicz et al., 2021). The oceanic crust of this basin must have been obducted already by the late Frasnian time since the Bardo Basin onlaps part of the Central Sudetic Ophiolite (Nowa Ruda Massif, e.g., Bederke, 1924; Mazur, 1987). Consequently, the metamorphic substratum of the Bardo Basin must have been exhumed and consolidated by the Late Devonian time. Detritus from the Góry Sowie Massif had been delivered to the inner Bardo Ocean from early Viséan (Haydukiewicz, 1990) or late Tournaisian (Wajsprych, 1995) onwards, constraining the time the basement units framing the basin were eventually exhumed to the surface.

Although the Central Sudetic Ocean was closed in the Late Devonian, deposition in the Saxothuringian Ocean, outboard of the Saxothuringian Terrane, continued until the latest Devonian or earliest Carboniferous as shown by paleontological evidence from the Kaczawa Unit (Baranowski et al., 1990) and the Bardo Basin (Haydukiewicz 1990, 1998; this study). Both units, despite dissimilar tectonic history and geological setting, comprise remnants of Paleozoic pre-Variscan basins containing fragments of lower Paleozoic–Devonian deep marine sediments. Conversely, the inner Bardo Basin hosted relatively shallow water sedimentation until the late Viséan (334 ± 3 Ma, Kryza et al., 2011; Paprotnia Beds). Only afterwards, sedimentation changed to hemipelagic with deposition of extensive flysch and wild-flysch series and emplacement of olistostromes (Wajsprych, 1978, 1986, 1995). Consequently, it is unlikely that the Famennian deep marine sediments described here, along with other Devonian and early Paleozoic olistoliths, were initially deposited in the present-day Bardo Basin. Even assuming substantial post-Variscan erosion, the coexistence of shallow- and deep-water facies in the latest Devonian would require a basin several orders of magnitude larger than its present size. Furthermore, all rocks older than Givetian would not have avoided regional metamorphism. Therefore, we propose that all deep-water pre-Carboniferous lithologies, possibly along with some Lower Carboniferous flysch sequences (Wajsprych 1986, 2008), were delivered to the Bardo Basin through gravitational sliding from the outer oceanic basin at the end of Early Carboniferous.

The presence of pyroclastic interbeds in the Famennian strata that have a continental arc geochemical signature indicates a possible link to a continental magmatic arc, the remnant of which is preserved within the Vrbno Group of the East Sudetes, ~80 km SE of the Bardo Basin (Patočka and Valenta, 1996; Janoušek et al., 2014; Figs. 15 and S4/3). The low-grade volcano-sedimentary complex of the Devonian Vrbno Group, up to 3000 m thick, occurs in two ~NE-SW–trending belts, separated by tectonic slices of the Cadomian para-autochthon (Janoušek et al., 2014). The basic-intermediate lavas of the calc-alkaline Western Volcanic Belt came from a moderately depleted mantle ($^{370}\varepsilon$Nd ~+3). Rare rhyolites (374.0 ± 1.7 Ma) were derived most likely from immature crust or by extensive fractionation of primary basaltic melts. This rock association is interpreted as a vestige of a deeply dissected continental arc (Janoušek et al., 2014; Figs. 17 and 18). The Eastern Volcanic Belt mainly consists of contemporaneous (371.0 ± 1.4 Ma) felsic alkaline lavas with geochemical signatures typical of a

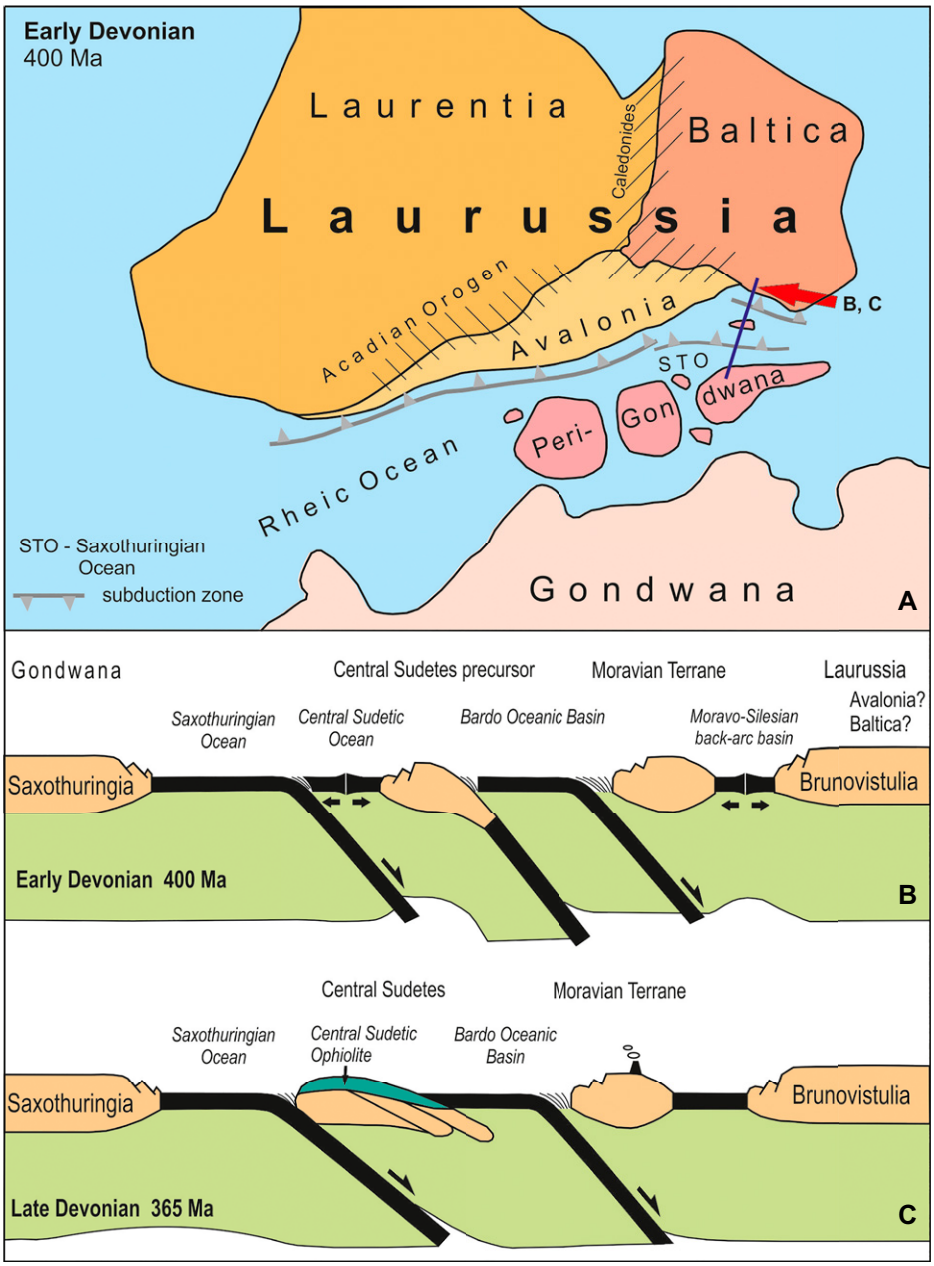

Figure 17. Hypothetical, simplified scenario of geodynamic evolution of the Sudetes of SW Poland in Devonian times (modified from Mazur et al., 2006). The arrow points to a line showing approximate location of conceptual cross-sections B–C, in which no major strike-slip displacements oriented at a high angle to these sections are considered. The Central Sudetes, including the Góry Sowie Massif are formed of continental crust with the Gondwana affinity that was partly subducted to mantle depths (B) and, subsequently, exhumed in a nappe pile during the Late Devonian (C). The Bardo oceanic tract was separated from the Saxothuringian Ocean by the Central Sudetic continental domain and remained an open oceanic basin until the latest Devonian (C) as documented by deep marine sediments of that age (see Fig. 18). Subduction of the Bardo section of the Saxothuringian Ocean (C) supports the volcanic arc being the precursor to the Vrbno Group of the East Sudetes.

within-plate igneous setting. The petrology and Nd-Sr isotopic data point to anatexis of a young metagranitic crust, resembling the Cadomian (Brunovistulian) basement (Janoušek et al., 2014). The associated metasediments comprise a succession of predominantly deep-water siliciclastic, siliceous, and calcareous slates. Paleontologic dating of crystalline limestones suggests that much of the Vrbno volcano-sedimentary succession was deposited between end Givetian and latest Frasnian times (Hladil, 1986). Although the pyroclastic horizons dated at Bardo are somewhat younger (middle Famennian) than the Vrbno Group (i.e., early Famennian at best; Fig. 8), scarce isotopic, elemental (Figs. 15B–D and S4/3B), and paleontological data from the latter possibly allow for a wider time span of eruptive activity, expected especially in the western belt.

The similarity to the Bavarian facies and the Kaczawa Unit suggests that the Bardo allochthonous succession represents the Saxothuringian Ocean that was eventually closed at the transition from Devonian to Carboniferous (Franke and Żelaźniewicz, 2000; Mazur and Aleksandrowski, 2001; Franke et al., 2017). In contrast to the other settings, the outer Bardo Ocean succession avoided regional metamorphism and erosion, providing unique information on the environmental conditions established in this ancient oceanic basin at the end of the Devonian. The Bardo cherty sediments studied here give an exceptional opportunity to look into paleoenvironmental proxies and reconstruct the hemipelagic facies evolution (Fig. 16) in the ocean that preceded accretion of the Variscan belt, information lost elsewhere due to a pervasive tectonic and metamorphic overprint. The Bardo Basin may have been preserved owing to its possible pull-apart origin that was related to synsedimentary activity of the Intrasudetic Fault (Franke et al., 1993).

Paleogeography of the Saxothuringian Ocean

The general facies architecture of the Bardo Basin shows its western polarity (Wajsprych, 1995, 2008), in agreement with a general WNW-ward polarity of the Central and West Sudetes (e.g., Mazur et al., 2006). Paleogeographic reconstruction of this convergent margin is hindered by the allochthonous position of the Vrbno volcanic arc (Moravian Terrane, Fig. 17) and general E-W shortening of the Sudetic orogenic wedge (Mazur et al., 2015). On the whole, the Saxothuringian Ocean was subducted beneath the western margin (present-day coordinates) of the Brunovistulian Terrane that was already amalgamated with Laurussia in Devonian time (Belka et al., 2002). The original locus of an active margin remains unknown since the western margin of the Brunovistulian Terrane is composed of mostly allochthonous units (Moravo-Silesian Zone). In the Early Devonian, the subduction zone was jammed by a peri-Gondwana microcontinent, being a precursor to the Góry Sowie Massif and Kłodzko Unit and jumped farther west (Fig. 17).

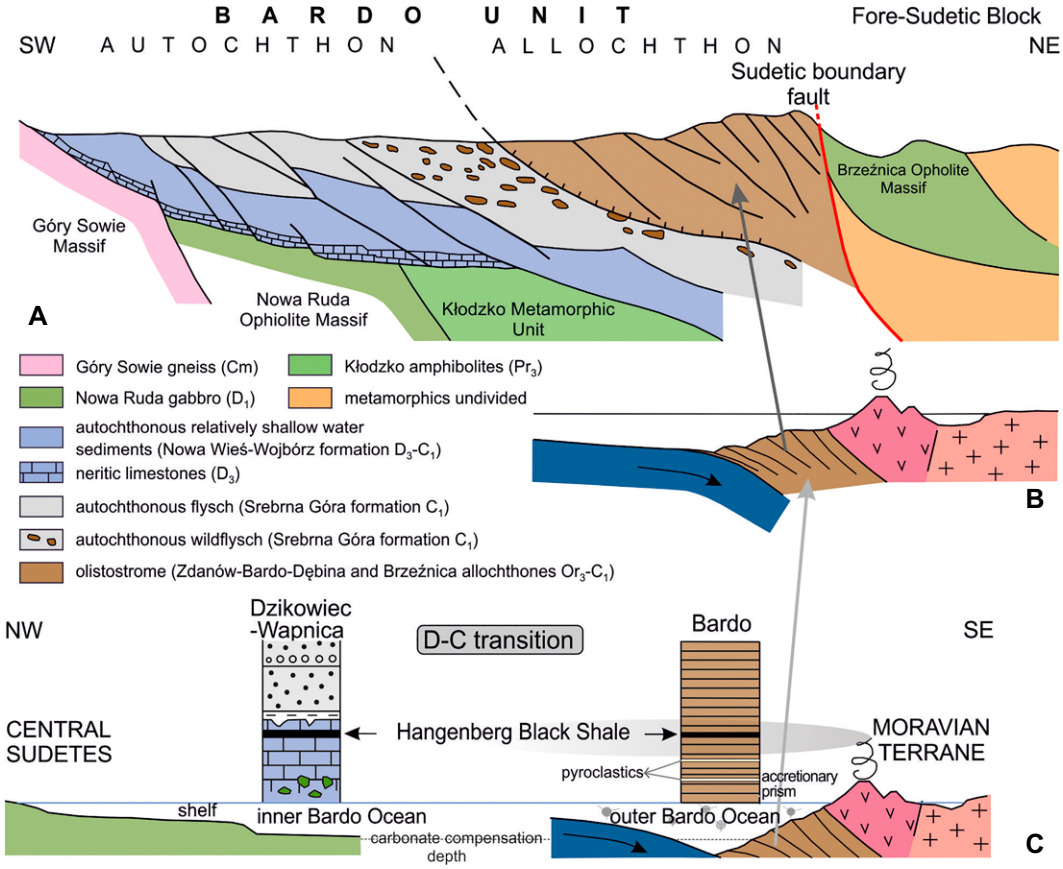

Figure 18. Synthetic tectonostratigraphic architecture of the Bardo Basin of SW Poland modified from Wajsprych (2008). (A) Conceptual NE-SW section through the basin showing westward shallowing. (B) Tectonic setting for accretion of the allochthonous succession of the Bardo Basin. (C) Model of the latest Devonian Bardo Basin, modified from Wajsprych (1986; 2008, their fig. 3A), with different facies recorded during the Devonian-Carboniferous (D–C) transition in the inner (after Matyja et al., 2021, their fig. 13) and outer settings.

However, eastward subduction beneath the Brunovistulian margin still continued, as evidenced by the Vrbno Group volcanic arc and pyroclastic inliers in the Bardo Basin. The section of the Saxothuringian Ocean parental to the Bardo allochthonous succession (outer Bardo Ocean herein; Fig. 18) was eventually shortened and uplifted during continental collision between the Saxothuringian Terrane, Central Sudetes, and Brunovistulian terrane, in the earliest Carboniferous (Mazur and Aleksandrowski, 2001; Konopásek et al., 2019).

CONCLUSIONS

(1) The Al-bentonite-rich cherty-clayey middle to late Famennian succession at Bardo offers an exceptional opportunity to look into the lost ocean that preceded accretion of the Variscan belt in the Central Sudetes. We documented the evolving depositional regimes in the hemipelagic Bardo Basin, with distinctive oceanic attributes such as fluctuating but mostly oligotrophic regimes and low primary production levels influenced by weak upwellings below the perennial oxygen minimum zone.

(2) The Hangenberg Black Shale has been identified in the Bardo oceanic setting in accordance with many characteristics known worldwide, such as anoxia, high productivity, warming, and volcanogenic mercury enrichment. A tectonic uplift of the source area near the D-C boundary, recorded by the distinguished felsic provenance signal of old continental crust, was paired with a global transgression in the interglacial episode.

(3) The distal record of Famennian explosive volcanic activity in the Bardo Ocean basin is likely related to a continental magmatic arc the remnant of which is preserved as the Vrbno Group of the East Sudetes. On the other hand, the Vrbno volcanism spans the Frasnian-Famennian boundary interval and may have contributed to the biotic crisis (see discussion in Racki, 2020).

(4) The allochthonous sediments from the Bardo Unit are interpreted as part of an accretionary prism that was gravitationally redeposited into the late orogenic basin in front of advancing Variscan nappes. The "lost" outer Bardo Ocean is thought to represent a tract of the waning Saxothuringian Ocean in the Peri-Gondwanan paleogeographic domain that was eventually subducted beneath the Brunovistulian margin of Laurussia.

ACKNOWLEDGMENTS

The study presents results of the MAESTRO grant 2013/08/A/ST10/00717 from the National Science Centre of Poland (to Grzegorz Racki) and the Polish Geological Institute-National Research Institute project number 62.9012.1903.00.0 (to Katarzyna Narkiewicz). We would like to thank Mariusz Paszkowski for his invaluable help as an initiator and guide in the two-stage field work in 2017, in which Katarzyna Sobień and Józef Kaźmierczak also participated. Michał Rakociński kindly provided unpublished geochemical data for the Dzikowiec locality in SW Poland and participated in field work in 2020. Zuzanna Wawrzyniak and Arkadiusz Krzątała helped in chemical preparation of chert samples and their photography, respectively. Discussions with Mariusz Paszkowski and Józef Kaźmierczak were stimulating for geological and environmental aspects, while Carlo Corradini kindly consulted about some conodont taxonomy problems. We especially thank two anonymous journal reviewers for their thorough reviews. Publication fee was partly subsidized by The National Fund for Environmental Protection and Water Management (Poland).

REFERENCES CITED

Adachi, M., Yamamoto, K., and Sugisaki, R., 1986, Hydrothermal chert and associated siliceous rocks from the northern Pacific: Their geological significance and indication of ocean ridge activity: Sedimentary Geology, v. 47, p. 125–148, https://doi.org/10.1016/0037-0738(86)90075-8.

Aleksandrowski, P., Kryza, R., Mazur, S., Pin, C., and Zalasiewicz, J.A., 1999, 2000, The Polish Sudetes: Caledonian or Variscan?: Transactions of the Royal Society of Edinburgh, v. 90, p. 127–146, https://doi.org/10.1017/S0263593300007197.

Algeo, T.J., and Liu, J., 2020, A re-assessment of elemental proxies for paleoredox analysis: Chemical

Geology, v. 540, no. 119549, https://doi.org/10.1016/j.chemgeo.2020.119549.

Aretz, M., 2020, Late Devonian extinctions, *in* Alderton, D., and Elias, S.A., eds., Encyclopedia of Geology (Second Edition), p. 628–636, https://doi.org/10.1016/B978-0-12-409548-9.12453-4 .

Aretz, M., Corradini, C., and Denayer, J., 2021, The Devonian-Carboniferous Boundary around the globe: A complement: Palaeobiodiversity and Palaeoenvironments, v. 101, p. 633–662, https://doi.org/10.1007/s12549-021-00495-y.

Armstrong-Altrin, J.S., and Verma, S.P., 2005, Critical evaluation of six tectonic setting discrimination diagrams using geochemical data of Neogene sediments from known tectonic settings: Sedimentary Geology, v. 177, p. 115–129, https://doi.org/10.1016/j.sedgeo.2005.02.004.

Awdankiewicz, M., Kryza, R., Turniak, K., Ovtcharova, M., and Schaltegger, U., 2021, The Central Sudetic Ophiolite (European Variscan Belt): Precise U-Pb zircon dating and geotectonic implications: Geological Magazine, v. 158, p. 555–566, https://doi.org/10.1017/S0016756820000722.

Baranowski, Z., Haydukiewicz, A., Kryza, R., Lorenc, S., Muszyński, A., Solecki, A., and Urbanek, Z., 1990, Outline of the geology of the Góry Kaczawskie (Sudetes, Poland): Neues Jahrbuch für Geologie und Paläontologie. Abhandlungen, v. 179, p. 223–257.

Barrett, T.J., 1981, Chemistry and mineralogy of Jurassic bedded chert overlying ophiolites in the North Apennines, Italy: Chemical Geology, v. 34, p. 289–317, https://doi.org/10.1016/0009-2541(81)90118-2.

Batten, D.J., 1996, Palynofacies and Palaeoenvironmental Interpretation, *in* Jansonius, J., and McGregor, D.C., eds., Palynology: Principles and applications: American Association of Stratigraphic Palynologists Foundation: Texas, USA, College Station, v. 3, p. 1011–1064.

Becker, R.T., Marshall, J.E.A., and Da Silva, A.C., 2020, The Devonian Period, *in* Gradstein, F.M., Ogg, J.G., Schmitz, M., and Ogg, G.M., eds., The Geologic Time Scale 2020: Amsterdam, Netherlands, Elsevier, v. 2, p. 733–810, https://doi.org/10.1016/B978-0-12-824360-2.00022-X.

Bederke, E., 1924, Das Devon in Schlesien und das Alter der Sudeten-faltung: Fortschritte der Geologie und Paläontologie, v. 7, p. 1–55.

Bederke, E., 1929, Die Grenze von Ost- und Westsudeten und ihre Bedeutung für die Einordnung der Sudeten in den Gebirgsbau Mitteleuropas: Geologische Rundschau, v. 20, p. 186–205, https://doi.org/10.1007/BF01805452.

Belka, Z., Valverde-Vaquero, P., Dörr, W., Ahrendt, H., Wemmer, K.M., Franke, W., and Schäfer, J., 2002, Accretion of first Gondwana-derived terranes at the margin of Baltica, *in* Winchester, J., Pharaoh, T., and Verniers, J., eds., Palaeozoic Amalgamation of Central Europe: Geological Society, London, Special Publication 201, p. 19–36, https://doi.org/10.1144/GSL.SP.2002.201.01.02.

Bennett, W.W., and Canfield, D.E., 2020, Redox-sensitive trace metals as paleoredox proxies: A review and analysis of data from modern sediments: Earth-Science Reviews, v. 204, no. 103175, https://doi.org/10.1016/j.earscirev.2020.103175.

Boström, K., 1983, Genesis of ferromanganese deposits: Diagnostic criteria for recent and old deposits, *in* Rona, P.A., Boström, K., Laubier, L., and Smith, K.L., eds., Hydrothermal Processes at Seafloor Spreading Centers: New York, Plenum, p. 473–489, https://doi.org/10.1007/978-1-4899-0402-7_20.

Branson, E.B., and Mehl, M.G., 1934, Conodonts from the Grassy Shale of Missouri: University of Missouri Studies, v. 8, p. 172–259.

Calvert, S.E., and Pedersen, T.F., 2007, Elemental proxies for palaeoclimatic and palaeoceanographic variability in marine sediments: Interpretation and application: Developments in Marine Geology, v. 1, p. 567–644, https://doi.org/10.1016/S1572-5480(07)01019-6.

Cecil, C.B., 2015, Paleoclimate and the origin of Paleozoic chert: Time to re-examine the origins of chert in the rock record: Sedimentary Record, v. 13, no. 3, p. 4–10, https://doi.org/10.2110/sedred.2015.3.4.

Chorowska, M., Milewicz, J., and Radlicz, K., 1992, Famennian and Tournaisian deposits from the Zdanów IG 1 borehole (Sudetes): Geological Quarterly, v. 36, p. 1–32.

Craigie, N., 2018, Principles of elemental chemostratigraphy: A practical user guide: Cham, Switzerland, Springer, 189 p., https://doi.org/10.1007/978-3-319-71216-1.

Cressman, E.R., 1962, Nondetrital siliceous sediments, *in* Fleischer, M., ed., Data of Geochemistry, Sixth Edition: Geological Survey Professional Paper 440-T, p. 1–23.

Cullers, R.L., 2000, The geochemistry of shales, siltstones and sandstones of Pennsylvanian-Permian age, Colorado, USA: Implications for provenance and metamorphic studies: Lithos, v. 51, p. 181–203, https://doi.org/10.1016/S0024-4937(99)00063-8.

Cymerman, Z., Badura, J., and Ihnatowicz, A., 2015, Objaśnienia do Szczegółowej Mapy Geologicznej Polski 1:50,000, Arkusz Nowa Ruda (868): Warszawa, Poland, Ministerstwo Środowiska, 100 p.

Derkowski, A., and Marynowski, L., 2018, Binding of heavy metals by oxidised kerogen in (palaeo)weathered black shales: Chemical Geology, v. 493, p. 441–450, https://doi.org/10.1016/j.chemgeo.2018.06.025.

De Wever, P., Dumitrica, P., Caulet, J.P., Nigrini, C., and Caridroit, M., 2001, Radiolarians in the Sedimentary Record: Boca Raton, Florida, USA, CRC Press, 533 p., https://doi.org/10.1201/9781482283181.

Dickinson, W.R., 2000, Geodynamic interpretation of Paleozoic tectonic trends in oriented oblique to the Mesozoic Klamath-Sierran continental margin in California, *in* Soreghan, M.J., and Gehrels, G.E., eds., Paleozoic and Triassic Paleogeography and Tectonics of Western Nevada and Northern California: Geological Society of America Special Paper 347, p. 209–245, https://doi.org/10.1130/0-8137-2347-7.209.

Dong, T., Harris, N.B., and Ayranci, K., 2018, Relative sea-level cycles and organic matter accumulation in shales of the Middle and Upper Devonian Horn River Group, northeastern British Columbia, Canada: Insights into sediment flux, redox conditions, and bioproductivity: Geological Society of America Bulletin, v. 130, p. 859–880, https://doi.org/10.1130/B31851.1.

Ferriday, T., and Montenari, M., 2016, Chemostratigraphy and chemofacies of source rock analogues: A high-resolution analysis of black shale successions from the Lower Silurian Formigoso Formation (Cantabrian Mountains, NW Spain): Stratigraphy & Timescales, v. 1, p. 123–255, https://doi.org/10.1016/bs.sats.2016.10.004.

Filipiak, P., and Racki, G., 2010, Proliferation of abnormal palynoflora during the end-Devonian biotic crisis: Geological Quarterly, v. 54, p. 1–14.

Floyd, P.A., and Leveridge, B.E., 1987, Tectonic environments of the Devonian Gramscatho basin, south Cornwall: Framework mode and geochemical evidence from turbidite sandstones: Journal of the Geological Society, v. 144, p. 531–542, https://doi.org/10.1144/gsjgs.144.4.0531.

Francovschi, I., Grădinaru, E., Roban, R.D., Ducea, M.N., Ciobotaru, V., and Leonid Shumlyanskyy, L., 2020, Rare earth element (REE) enrichment of the late Ediacaran Kalyus Beds (East European Platform) through diagenetic uptake: Geochemistry, v. 80, no. 2, https://doi.org/10.1016/j.chemer.2020.125612.

Franke, W., and Żelaźniewicz, A., 2000, The eastern termination of the Variscides: Terrane correlation and kinematic evolution, *in* Franke, W., Haak, V., Oncken, O., and Tanner, D., eds., Orogenic Processes: Quantification and Modelling in the Variscan Belt: Geological Society, London, Special Publication 179, p. 63–86, https://doi.org/10.1144/GSL.SP.2000.179.01.06.

Franke, W., Żelaźniewicz, A., Porebski, S.J., and Wajspyrch, B., 1993, Saxothuringian zone in Germany and Poland: Differences and common features: Geologische Rundschau, v. 82, p. 583–599, https://doi.org/10.1007/BF00212418.

Franke, W., Dallmeyer, R.D., and Weber, K., 1995, Geodynamic Evolution, *in* Dallmeyer, R.D., Franke, W., and Weber, K., eds., Pre-Permian geology of Central and Eastern Europe: Berlin, Germany, Springer, p. 579–593, https://doi.org/10.1007/978-3-642-77518-5_57.

Franke, W., Cocks, L.R.M., and Torsvik, T.H., 2017, The Palaeozoic Variscan oceans revisited: Gondwana Research, v. 48, p. 257–284, https://doi.org/10.1016/j.gr.2017.03.005.

Fraser, T.A., and Hutchison, M.P., 2017, Lithogeochemical characterization of the Middle–Upper Devonian Road River Group and Canol and Imperial formations on Trail River, east Richardson Mountains, Yukon: Age constraints and a depositional model for fine-grained strata in the Lower Paleozoic Richardson trough: Canadian Journal of Earth Sciences, v. 54, p. 731–765, https://doi.org/10.1139/cjes-2016-0216.

Gao, P., He, Z., Lash, G.G., Qin, Z., and Xiao, Y., 2021, Controls on silica enrichment of Lower Cambrian organic-rich shale: Marine and Petroleum Geology, v. 130, no. 105126, p. 1–14, https://doi.org/10.1016/j.marpetgeo.2021.105126.

German, C.R., and Von Damm, K.L., 2006, Hydrothermal processes, *in* Holland, H.G., and Turekian, K.K., eds., The Treatise on Geochemistry: Amsterdam, Netherlands, Elsevier, v. 6, p. 45–85.

Girty, G., Ridge, D., Knaack, C., Johnson, D., and Al-Riyami, R., 1996, Provenance and depositional setting of Paleozoic chert and argillite, Sierra Nevada, California: Journal of Sedimentary Research, v. 66, p. 107–118, https://doi.org/10.1306/D42682CA-2B26-11D7-8648000102C1865D.

Golonka, J., 2020, Late Devonian paleogeography in the framework of global plate tectonics: Global and Planetary Change, v. 186, no. 103129, https://doi.org/10.1016/j.gloplacha.2020.103129.

Grasby, S.E., Them, T.R., Chen, Z., Yin, R.S., and Ardakani, O.H., 2019, Mercury as a proxy for volcanic emissions in the geologic record: Earth-Science Reviews, v. 196, no. 102880, https://doi.org/10.1016/j.earscirev.2019.102880.

Grenne, T., and Slack, J.F., 2005, Geochemistry of jasper beds from the Ordovician Løkken ophiolite, Norway: Origin of proximal and distal siliceous exhalates: Economic Geology and the Bulletin of the Society of Economic Geologists, v. 100, p. 1511–1527, https://doi.org/10.2113/gsecongeo.100.8.1511.

Guillong, M., von Quadt, A., Sakata, S., Peytcheva, I., and Bachmann, O., 2014, LA-ICP-MS Pb-U dating of young zircons from the Kos-Nisyros volcanic centre, SE Aegean arc: Journal of Analytical Atomic Spectrometry, v. 29, p. 963–970, https://doi.org/10.1039/C4JA00009A.

Gunia, T., 1985, Pozycja geologiczna bloku sowiogórskiego i jego wpływ na paleogeografię paleozoiku Sudetów środkowych: Geologia Sudetica, v. 20, p. 83–119.

Gursky, H.J., 1996, Siliceous rocks of the Culm Basin, Germany, *in* Strogen, P., Somerville, I.D., and Jones, G.L., eds., Recent Advances in Lower Carboniferous Geology: Geological Society, London, Special Publication 107, p. 303–314, https://doi.org/10.1144/GSL.SP.1996.107.01.21.

Harris, N.B., McMillan, J.M., Knapp, L.J., and Mastalerz, M., 2018, Organic matter accumulation in the Upper Devonian Duvernay Formation, Western Canada Sedimentary Basin, from sequence stratigraphic analysis and geochemical proxies: Sedimentary Geology, v. 376, p. 185–203, https://doi.org/10.1016/j.sedgeo.2018.09.004.

Hartenfels, S., 2011, Die globalen Annulata-Events und die Dasberg-Krise (Famennium, Oberdevon) in Europa und Nord-Afrika: Hochauflösende Conodonten-Stratigraphie,Karbonat-Mikrofazies, Paläoökologie und Paläodiversität: Münstersche Forschungen zur Geologie und Paläontologie, v. 105, p. 17–527.

Haydukiewicz, J., 1979, Stratigraphy of the Zdanow series in the northern part of the Bardo unit on the basis of conodonts: Geologia Sudetica, v. 14, p. 77–99.

Haydukiewicz, J., 1990, Stratigraphy of Paleozoic rocks of the Gory Bardzkie and some remarks on their sedimentation (Poland): Neues Jahrbuch für Geologie und Paläontologie: Abhandlungen, v. 17, p. 275–284.

Haydukiewicz, J., 1998, Latest Devonian conodonts from an olistolith in the northern part of the Góry Bardzkie: West Sudetes: Geologia Sudetica, v. 31, p. 61–68.

Haydukiewicz, J., 2002, Thermal alteration of conodonts in Devonian to Lower Carboniferous rocks of the Góry Bardzkie: Acta Universitatis Wratislaviensis: Prace Geologiczno-Mineralogiczne, v. 72, p. 7–30.

Hein, J.R., and Parrish, J.R., 1987, Distribution of siliceous deposits in time and space, *in* Hein, J.R., ed., Siliceous Sedimentary Rock-Hosted Ores and Petroleum: New York, USA, Van Nostrand Reinhold, p. 10–57.

Helms, J., 1959, Conodonten aus dem Saalfelder Oberdevon (Thuringen): Geologie, v. 8, p. 634–677.

Higgs, K., Clayton, G., and Keegan, B.J., 1988, Stratigraphic and systematic palynology of the Tournaisian rocks of Ireland: Geological Survey of Ireland Special Paper 7, p. 1–93.

Hladil, J., 1986, Trends in the development and cyclic patterns of Middle and Upper Devonian build-ups: Facies, v. 15, p. 1–33, https://doi.org/10.1007/BF02536716.

Hladil, J., Mazur, S., Galle, A., and Ebert, J., 1999, Revised age of the Mały Bożków limestone in the Kłodzko metamorphic unit (early Givetian, late Middle Devonian): Implications for the geology of the Sudetes: Neues Jahrbuch für Geologie und Paläontologie, Abhandlungen, v. 211, p. 329–353, https://doi.org/10.1127/njgpa/211/1999/329.

Hou, Q., Mou, C., Han, Z., Ge, X., and Wang, O., 2021, Origin of chert in the Upper Ordovician–Lower Silurian: Implications for the sedimentary environment of North Qilian Orogen: Earth and Environmental Science Transactions of the Royal Society of Edinburgh, v. 112, p. 13–28, https://doi.org/10.1017/S1755691021000025.

Huff, W.D., 2016, K-bentonites: A review: The American Mineralogist, v. 101, p. 43–70, https://doi.org/10.2138/am-2016-5339.

Hüneke, H., and Henrich, R., 2011, Pelagic sedimentation in modern and ancient oceans, *in* Hüneke, H., and Mulder, T., eds., Deep-Sea Sediments: Developments in Sedimentology, v. 63, p. 215–351, https://doi.org/10.1016/B978-0-444-53000-4.00004-4.

Janoušek, V., Aichler, J., Hanžl, P., Gerdes, A., Erban, V., Žáček, V., Pecina, V., Pudilová, M., Hrdličková, K., Mixa, P., and Žáčková, E., 2014, Constraining genesis and geotectonic setting of metavolcanic complexes: A multidisciplinary study of the Devonian Vrbno Group (Hrubý Jeseník Mts., Czech Republic): International Journal of Earth Sciences, v. 103, p. 455–483, https://doi.org/10.1007/s00531-013-0975-4.

Jones, D.L., and Murchey, B., 1986, Geologic significance of Paleozoic and Mesozoic radiolarian chert: Annual Review of Earth and Planetary Sciences, v. 14, p. 455–492, https://doi.org/10.1146/annurev.ea.14.050186.002323.

Jones, M.T., Percival, L.M.E., Stokke, E.W., Frieling, J., Mather, T.A., Riber, L., Schubert, B.A., Schultz, B., Tegner, C., Planke, S., and Svensen, S.H., 2019, Mercury anomalies across the Palaeocene–Eocene Thermal Maximum: Climate of the Past, v. 15, p. 217–236, https://doi.org/10.5194/cp-15-217-2019.

Kaiser, S.I., Aretz, M., and Becker, R.T., 2016, The global Hangenberg Crisis (Devonian–Carboniferous transition): Review of a first-order mass extinction, *in* Becker, R.T., Königshof, P., and Brett, C.E., eds., Devonian Climate, Sea Level and Evolutionary Events: Geological Society of London, Special Publication 423, p. 387–437, https://doi.org/10.1144/SP423.9.

Kedo, G.I., 1974, New species of spores from the Upper Devonian of the Pripyat Depression [in Russian], *in* Spory Paleozoya Belorussii (Pripyatskaya Vpadina): Minsk, Balarus, Soviet Union, Belorussian Geological Prospecting Research Institute Collected Papers, p. 3–72.

Ketris, M.P., and Yudovich, Y.E., 2009, Estimations of Clarkes for carbonaceous biolithes: World averages for trace element contents in black shales and coals: International Journal of Coal Geology, v. 78, p. 135–148, https://doi.org/10.1016/j.coal.2009.01.002.

Khan, M.Z., Feng, O., Zhang, K., and Guo, W., 2019, Biogenic silica and organic carbon fluxes provide evidence of enhanced marine productivity in the Upper Ordovician-Lower Silurian of South China: Palaeogeography, Palaeoclimatology, Palaeoecology, v. 534, no. 109278, https://doi.org/10.1016/j.palaeo.2019.109278.

Kiessling, W., and Tragelehn, H., 1994, Devonian radiolarian faunas of conodont-dated localities in the Frankenwald (Northern Bavaria, Germany): Abhandlungen der geologisches Bundesanstalt in Wien, v. 50, p. 219–255.

Kiipli, T., 2021, Silurian volcanism recorded in sedimentary sections at the southwestern margin of the East European Platform: Geochemical correlation and tectonomagmatic interpretation: Geological Quarterly, v. 65, https://doi.org/10.7306/gq.1580.

Kiipli, T., Hints, R., Kallaste, T., Nielsen, A.T., Pajusaar, S., and Schovsbo, N.H., 2020, Tectono-magmatic division of the Late Ordovician (Sandbian) volcanism at the south-western margin of Baltica using immobile trace elements: Relations to the plate movements in the Iapetus Palaeo-Ocean: Geological Journal, v. 55, p. 5155–5165, https://doi.org/10.1002/gj.3737.

Konopásek, J., Anczkiewicz, R., Jeřábek, P., Corfu, F., and Žáčková, E., 2019, Chronology of the Saxothuringian subduction in the West Sudetes (Bohemian Massif, Czech Republic and Poland): Journal of the Geological Society, v. 176, p. 492–504, https://doi.org/10.1144/jgs2018-173.

Kremer, B., 2020, Entrapment and transformation of post-bloom radiolarians in cyanobacterial mats as a factor enhancing the formation of black cherts in the Early Silurian sea: Journal of Sedimentary Research, v. 90, p. 151–164, https://doi.org/10.2110/jsr.2020.7.

Kremer, B., and Kazmierczak, J., 2005, Cyanobacterial mats from Silurian black radiolarian cherts: phototrophic life at the edge of darkness?: Journal of Sedimentary Research, v. 75, p. 897–906, https://doi.org/10.2110/jsr.2005.069.

Kryza, R., Mazur, S., and Aleksandrowski, P., 1999, Pre-Late Devonian unconformity in the Kłodzko area excavated: A record of Eo-Variscan metamorphism and exhumation in the Sudetes: Geologia Sudetica, v. 32, p. 127–137.

Kryza, R., Mazur, S., and Oberc-Dziedzic, T., 2004, The Sudetic geological mosaic: Insights into the root of the Variscan orogeny: Przegląd Geologiczny, v. 52, p. 761–773.

Kryza, R., Muszer, J., Haydukiewicz, J., August, C., Jurasik, M., and Rodionov, N., 2011, A SIMS zircon age for a biostratigraphically dated Upper Viséan (Asbian) bentonite in the Central-European Variscides (Bardo Unit, Polish Sudetes): International Journal of Earth Sciences, v. 100, p. 1227–1235, https://doi.org/10.1007/s00531-010-0529-y.

Kuroda, J., Ihoriya, N., Hori, R.S., Ogawa, N.O., Ikehara, M., Tanimizu, M., and Ohkouchi, N., 2015, Geochemistry of Aptian bedded chert succession from the deep Pacific basin: New insights into Cretaceous oceanic anoxic event (OAE) 1a, *in* Neal, C.R., Sager, W.W., Sano, T., and Erba, E., eds., The Origin, Evolution, and Environmental Impact of Oceanic Large Igneous Provinces: Geological Society of America Special Paper 511, p. 305–328, https://doi.org/10.1130/2015.2511(16).

Lash, G.G., 2017, A multiproxy analysis of the Frasnian-Famennian transition in western New York State, U.S.A: Palaeogeography, Palaeoclimatology, Palaeoecology, v. 473, p. 108–122, https://doi.org/10.1016/j.palaeo.2017.02.032.

Lazarus, D., Suzuki, N., Ishitani, Y., and Takahashi, K., 2020, Paleobiology of the Polycystine Radiolaria: Hoboken, New Jersey, USA, Wiley-Blackwell, 504 p.

Le Hérissé, A.L., Servais, T., and Wicander, R., 2000, Devonian acritarchs and related forms: Courier Forschungsinstitut Senckenberg, v. 220, p. 195–205.

Lei, Z., Dashtgard, S.E., Wang, J., Li, M., Feng, Q., Yu, Q., Zhao, A., and Du, L., 2019, Origin of chert in Lower Silurian Longmaxi Formation: Implications for tectonic evolution of Yangtze Block, South China: Palaeogeography, Palaeoclimatology, Palaeoecology, v. 529, p. 53–66, https://doi.org/10.1016/j.palaeo.2019.05.017.

Liao, Z.W., Hu, W.X., Fu, X.G., and Hu, Z.Y., 2019, Geochemistry of upper Permian siliceous rocks from the Lower Yangtze region, southeastern China: implications for the origin of chert and Permian ocean *chemistry*: Petroleum Science, v. 16, p. 252–266, https://doi.org/10.1007/s12182-018-0293-3.

Lo, F.L., Chen, H.F., and Fang, J.N., 2017, Discussion of suitable chemical weathering proxies in sediments by comparing the dissolution rates of minerals in different rocks: The Journal of Geology, v. 125, p. 83–99, https://doi.org/10.1086/689184.

Ma, K., Hinnov, L.A., Zhang, X., and Gong, Y., 2020, Astronomical time calibration of the Upper Devonian Lali section, SouthChina: Global and Planetary Change, v. 193, no. 103267, p. 1–13, https://doi.org/10.1016/j.gloplacha.2020.103267.

Marshall, J.E., Lakin, J., Troth, I. and Wallace-Johnson, S.M, 2020, UV-B radiation was the Devonian-Carboniferous boundary terrestrial extinctions kill mechanism: Science Advances, v. 6, p. 1–9, https://doi.org/10.1126/sciadv.aba0768.

Martin, R.E., and Servais, T., 2019, Did the evolution of the phytoplankton fuel the diversification of the marine biosphere?: Lethaia, v. 53, p. 5–31, https://doi.org/10.1111/let.12343.

Matyja, H., Woroncowa-Marcinowska, T., Filipiak, P., Brański, P., and Sobień, K., 2021, The Devonian/Carboniferous boundary interval in Poland: Multidisciplinary studies in pelagic (Holy Cross Mountains and Sudetes) and ramp (Western Pomerania) successions: Palaeobiodiversity and Palaeoenvironments, v. 101, p. 421–472, https://doi.org/10.1007/s12549-020-00442-3.

Maziane, N., Higgs, K., and Streel, M., 2002, Biometry and paleoenvironment of *Retispora lepidophyta* (Kedo) Playford 1976 and associated miospores in the latest Famennian nearshore marine facies, eastern Ardenne (Belgium): Review of Palaeobotany and Palynology, v. 118, p. 211–226, https://doi.org/10.1016/S0034-6667(01)00115-4.

Mazur, S., 1987, Tektonika utworów górnego dewonu i dolnego karbonu w kamieniołomie w Dzikowcu (Góry Bardzkie): Przegląd Geologiczny, v. 35, p. 327–332.

Mazur, S., and Aleksandrowski, P., 2001, The Tepla(?)/Saxothuringian suture in the Karkonosze–Izera massif, western Sudetes, central European Variscides: International Journal of Earth Sciences, v. 90, p. 341–360, https://doi.org/10.1007/s005310000146.

Mazur, S., Aleksandrowski, P., Kryza, J., and Oberc-Dziedzic, T., 2006, The Variscan Orogen in Poland: Geological Quarterly, v. 50, p. 89–118.

Mazur, S., Turniak, K., Szczepański, J., and McNaughton, N.J., 2015, Vestiges of Saxothuringian crust in the Central Sudetes, Bohemian Massif: Zircon evidence of a recycled subducted slab provenance: Gondwana Research, v. 27, p. 825–839, https://doi.org/10.1016/j.gr.2013.11.005.

McLennan, S.M., 2001, Relationships between the trace element composition of sedimentary rocks and upper continental crust: Geochemistry, Geophysics, Geosystems, v. 2, no. 4, https://doi.org/10.1029/2000GC000109.

McLennan, S.M., Hemming, S., McDaniel, D.K., and Hanson, G.N., 1993, Geochemical approaches to sedimentation, provenance and tectonics, *in* Johansson, M.J., and Basu, A., eds., Processes Controlling the Composition of Clastic Sediments: Geological Society of America Special Paper 284, p. 21–40, https://doi.org/10.1130/SPE284-p21.

Menor-Salván, C., Tornos, F., Fernández-Remolar, D., and Amils, R., 2010, Association between catastrophic paleovegetation changes during Devonian-Carboniferous boundary and the formation of giant massive sulfide deposits: Earth and Planetary Science Letters, v. 299, p. 398–408, https://doi.org/10.1016/j.epsl.2010.09.020.

Mikulski, S.Z., and Williams, I.S., 2014, Zircon U-Pb ages of granitoid apophyses in the western part of the Kłodzko-Złoty Stok Granite Pluton (SW Poland): Geological Quarterly, v. 58, p. 251–262, https://doi.org/10.7306/gq.1141.

Müller, K.J., 1956, Zur Kenntnis der Conodonten-Fauna des europaischen Devons, 1; Die Gattung *Palmatolepis*: Abhandlunghen and Senckenbergischen Naturforschenden Gesellschaft, v. 494, p. 1–70.

Murray, R.W., 1994, Chemical criteria to identify the depositional environment of chert: General principles and applications: Sedimentary Geology, v. 90, p. 213–232, https://doi.org/10.1016/0037-0738(94)90039-6.

Murray, R.W., Jones, D.L., and Buchholtz ten Brink, M.R., 1992, Diagenetic formation of bedded chert: Evidence from chemistry of the chert-shale couplet: Geology, v. 20, p. 271–274, https://doi.org/10.1130/0091-7613(1992)020<0271:DFOBCE>2.3.CO;2.

Nisbet, E.G., and Price, I., 1974, Siliceous turbidites: Bedded cherts as redeposited, ocean ridge-derived sediments, *in* Hsü, K.J., and Jenkyns,H.C., eds., Pelagic Sediments: On Land and Under the Sea: The International

Association of Sedimentologists Special Publication 1, p. 351–366.
Oberc, J., 1951, Przewodnik do wycieczek XXIV Zjazdu Polskiego Towarzystwa Geologicznego w Sudetach w r. 1951, Wycieczka B. Problematyka geologiczna Gór Bardzkich: Roczniki Polskiego Towarzystwa Geologicznego, v. 21, p. 415–451.
Oberc, J., 1957, Region Gór Bardzkich (Sudety). Przewodnik dla geologów: Warszawa, Poland, Wydawnictwa Geologiczne, 283 p.
Oberc, J., 1972, Budowa geologiczna Polski, v. 4, Tektonika, part 2, Sudety i obszary przyległe: Warszawa, Poland, Wydawnictwo Geologiczne, 307 p.
Oberc, J., 1980, Early to Middle Variscan development of the West Sudetes: Acta Geologica Polonica, v. 30, p. 27–52.
Oberc, J., Badura, J., Przybylski, B., and Jamrozik, L., 1994, Szczegółowa mapa geologiczna Sudetów w skali 1:25,000, arkusz Bardo Śląskie: Warszawa, Poland, Państwowy Instytut Geologiczny.
O'Brien, P.J., Kröner, A., Jaeckel, P., Hegner, E., Żelaźniewicz, A., and Kryza, R., 1997, Petrological and isotopic studies on Palaeozoic high pressure granulites with a medium pressure overprint, Góry Sowie Mts: Polish Sudetes: Journal of Petrology, v. 38, p. 433–456, https://doi.org/10.1093/petroj/38.4.433.
Oppenheimer, C., Fischer, T.P., and Scaillet, B., 2014, Volcanic degassing: Process and impact, *in* Holland, H.G., and Turekian, K.K., eds., Geochemistry of Earth Surface Systems: Treatise on Geochemistry: Elsevier, Amsterdam, Netherlands, v. 4, p. 111–179, https://doi.org/10.1016/B978-0-08-095975-7.00304-1.
Pacholska, A., 1978, On the tectonic breccias at southern edge of the Sowie Góry gneiss błock: Geologia Sudetica, v. 13, p. 41–63.
Patočka, F., and Valenta, J., 1996, Geochemistry of the Late Devonian intermediate to acid metavolcanic rocks from the southern part of the Vrbno Group, the Jeseniky Mts. (Moravo-Silesian Belt, Bohemian Massif, Czech Republic): Paleotectonic implications: Geolines (Praha), v. 4, p. 42–54.
Pearce, J.A., 1996, A User's Guide to Basalt Discrimination Diagrams, *in* Wyman, D.A., ed., Trace Element Geochemistry of Volcanic Rocks: Applications for Massive Sulphide Exploration: Geological Association of Canada, Short Course Notes 12, p. 79–113.
Pisarzowska, A., Rakociński, M., Marynowski, L., Szczerba, M., Thoby, M., Paszkowski, M., Perri, M.C., Spalletta, C., Schönlaub, H.-P., Kowalik, N., and Gereke, M., 2020, Large environmental disturbances caused by magmatic activity during the Late Devonian Hangenberg Crisis: Global and Planetary Change, v. 190, p. 1–24, https://doi.org/10.1016/j.gloplacha.2020.103155.
Playford, G., 1976, Plant microfossils from the Upper Devonian and Lower Carboniferous of the Canning Basin, Western Australia: Palaeontographica. Abteilung B, Paläophytologie, v. 158, p. 1–71.
Pointon, M.A., Chew, D.M., Delcambre, B., and Sevastopulo, G.D., 2018, Geochemistry and origin of Carboniferous (Mississippian; Viséan) bentonites in the Namur-Dinant Basin, Belgium: Evidence for a Variscan volcanic source: Geologica Belgica, v. 21, p. 1–17, https://doi.org/10.20341/gb.2017.011.
Porębska, E., 1982, Latest Silurian and Early Devonian graptolites from Żdanów section, Bardo Mts. (Sudetes): Annales Societatis Geologorum Poloniae, v. 52, p. 89–209.
Prajith, S., Abhishek, T.P., and Kurian, J., 2021, Geochemistry of core sediments from the southeastern Bay of Bengal: Inferences on weathering and early diagenetic changes: Geoscience Frontiers, v. 12, p. 495–504, https://doi.org/10.1016/j.gsf.2020.08.011.
Prestianni, C., Sautois, M., and Denayer, J., 2016, Disrupted continental environments around the Devonian-Carboniferous Boundary: Introduction of the *tener* event: Geologica Belgica, v. 19, p. 135–145, https://doi.org/10.20341/gb.2016.013.
Racki, G., 2020, A volcanic scenario for the Frasnian–Famennian major biotic crisis and other Late Devonian global changes: More answers than questions?: Global and Planetary Change, v. 189, p. 1–29, https://doi.org/10.1016/j.gloplacha.2020.103174.
Racki, G., and Cordey, F., 2000, Radiolarian palaeoecology and radiolarites: Is the present the key to the past?: Earth-Science Reviews, v. 52, p. 83–120, https://doi.org/10.1016/S0012-8252(00)00024-6.
Racki, G., Königshof, P., Belka, Z., Dopieralska, J., and Pisarzowska, A., 2019, Diverse depositional and geochemical signatures of the Frasnian-Famennian global event in western Thailand reveal Palaeotethyan vs. Western Australian geotectonic affinities: Journal of Asian Earth Sciences X, v. 2, p. 1–23, https://doi.org/10.1016/j.jaesx.2019.100010.
Ran, B., Liu, S.G., Jansa, L., Sun, W., Yang, D., Ye, Y.H., Wang, S.Y., Luo, C., Zhang, X., and Zhang, C.J., 2015, Origin of the Upper Ordovician–lower Silurian cherts of the Yangtze block, South China, and their palaeogeographic significance: Journal of Asian Earth Sciences, v. 108, p. 1–17, https://doi.org/10.1016/j.jseaes.2015.04.007.
Randon, C., and Caridroit, M., 2008, Age and origin of Mississippian lydites: Examples from the Pyrénées, southern France: Geological Journal, v. 43, p. 261–278, https://doi.org/10.1002/gj.1101.
Ratcliffe K. T, Wright AM, Montgomery P, Palfrey A, Vonk A, Vermeulen J, and Barrett M., 2010, Application of chemostratigraphy to the Mungaroo Formation, the Gorgon Field, offshore northwest Australia: The APPEA Journal, v. 50, p. 371–388, https://doi.org/10.1071/AJ09022.
Rejebian, V.A., Harris, A.G., and Huebner, J.S., 1987, Conodont color and textural alteration: An index to regional metamorphism, contact metamorphism and hydrothermal alteration: Geological Society of America Bulletin, v. 99, p. 471–479, https://doi.org/10.1130/0016-7606(1987)99<471:CCATAA>2.0.CO;2.
Riegel, W., 2008, The Late Palaeozoic phytoplankton blackout: Artefact or evidence of global change?: Review of Palaeobotany and Palynology, v. 148, p. 73–90, https://doi.org/10.1016/j.revpalbo.2006.12.006.
Romer, R.L., and Hahne, K., 2010, Life of the Rheic Ocean: Scrolling through the shale record: Gondwana Research, v. 17, p. 236–253, https://doi.org/10.1016/j.gr.2009.09.004.
Ronov, A.B., Yaroshevskiy, A.A., and Migdisov, A.A., 1991, Chemical constitution of the Earth's crust and geochemical balance of the major elements: International Geology Review, v. 33, p. 1049–1097, https://doi.org/10.1080/00206819109465737.
Rothwell, R.G., and Croudace, I.W., 2015, Twenty years of XRF core scanning marine sediments: What do geochemical proxies tell us? *in* Croudace, I.W., and Rothwell R.G., eds., Micro-XRF Studies of Sediment Cores Applications of a Non-destructive Tool for the Environmental Sciences: Dordrecht, Netherlands, Springer, p. 25–102, https://doi.org/10.1007/978-94-017-9849-5_2.
Rudnick, R.L., and Gao, S., 2003, The Composition of the Continental Crust, *in* Holland, H.D. and Turekian, K.K., eds., The Crust: Amsterdam, Netherlands, Treatise on Geochemistry: Elsevier, v. 3, p. 1–64, https://doi.org/10.1016/b0-08-043751-6/03016-4.
Sageman, B.B., and Lyons, T.W., 2003, Geochemistry of fine-grained sediments and sedimentary rocks, *in* Turekian, K, and Holland, H.D., eds., Treatise on Geochemistry: Amsterdam, Netherlands, Elsevier, v. 7, p. 115–158, https://doi.org/10.1016/B0-08-043751-6/07157-7.
Spalletta, C., Perri, M.C., Over, D.J., and Corradini, C., 2017, Famennian (Upper Devonian) conodont zonation: Revised global standard: Bulletin of Geosciences, v. 92, p. 31–57, https://doi.org/10.3140/bull.geosci.1623.
Streel, M., Higgs, K., Loboziak, S., Riegel, W., and Steemans, P., 1987, Spore stratigraphy and correlation with faunas and floras in the type marine Devonian of the Ardenne-Rhenish regions: Review of Palaeobotany and Palynology, v. 50, p. 211–229, https://doi.org/10.1016/0034-6667(87)90001-7.
Streel, M., Caputo, M.V., Loboziak, S., and Melo, J.H.G., 2000, Late Frasnian–Famennian climates based on palynomorph analyses and the question of the Late Devonian glaciations: Earth-Science Reviews, v. 52, p. 121–173, https://doi.org/10.1016/S0012-8252(00)00026-X.
Sweere, T., Sander van den, B., Dickson, A.J., and Reichart, G.J., 2016, Definition of new trace-metal proxies for the controls on organic matter enrichment in marine sediments based on Mn, Co, Mo and Cd concentrations: Chemical Geology, v. 441, p. 235–245, https://doi.org/10.1016/j.chemgeo.2016.08.028.
Tabaud, A.S., Štípská, P., Mazur, S., Schulmann, K., Míková, J., Wong, J., and Sun, M., 2021, Evolution of Cambro-Ordovician North Gondwana active margin: Geochemistry and zircon geochronology evidence from Góry Sowie metasedimentary rocks: Gondwana Research, v. 90, p. 1–26, https://doi.org/10.1016/j.gr.2020.10.011.
Taylor, S.R., and McLennan, S.M., 1985, The Continental Crust: Its Composition and Evolution: Oxford, UK, Blackwell, 312 p.
Tribovillard, N., Algeo, T.J., Lyons, T., and Riboulleau, A., 2006, Trace metals as paleoredox and paleoproductivity proxies: An update: Chemical Geology, v. 232, p. 12–32, https://doi.org/10.1016/j.chemgeo.2006.02.012.
Udchachon, M., Thassanapak, H.M., Feng, Q., and Burrett, C., 2017, Palaeoenvironmental implications of geochemistry and radiolarians from Upper Devonian chert/shale sequences of the Truong Son fold belt, Laos: Geological Journal, v. 52, p. 154–173, https://doi.org/10.1002/gj.2743.
Wajsprych, B., 1978, Allochtoniczne skały paleozoiczne w osadach wizeńskich Gór Bardzkich (Sudety) [Allochthonous Paleozoic rocks in the Visean of the Bardzkie Mts. (Sudetes)]: Rocznik Polskiego Towarzystwa Geologicznego, v. 48, p. 99–127.
Wajsprych, B., 1986, Sedimentary record of tectonic activity on a Devonian-Carboniferous active continental margin, Sudetes, *in* Teisseyre, A.K., ed., IAS 7th European Meeting Excursion Guidebook, Kraków-Poland: Wrocław, Poland, Ossolineum, p. 141–162.
Wajsprych, B., 1995, The Bardo Mts rock complex: The Famennian–Lower Carboniferous preflysch (platform)—to flysch (foreland) basin succession, the Sudetes, *in* Guide to Excursion B2 of XIII International Congress on Carboniferous–Permian, 29 August–2 September, Krakow, Poland: Warszawa, Państwowy Instytut Geologiczny, p. 23–42.
Wajsprych, B., 2008, The Bardo Mts. Rock Complex (BMRC) as a core of a concept of the Central Sudetes Geopark (SW Poland), *in* Solecki, A.T., ed., Geoeducational Potential of the Sudety Mts: Wrocław, Poland, Fundacja Ostoja, p. 101–112.
Walliser, O.H., 1996, Global events in the Devonian and Carboniferous, *in* Walliser, O.H., ed., Global Events and Event Stratigraphy in the Phanerozoic: Berlin, Springer, p. 225–250, https://doi.org/10.1007/978-3-642-79634-0_11.
Wang, Z., et al., 2020, Evaluating episodic hydrothermal activity in South China during the early Cambrian: Implications for biotic evolution: Marine and Petroleum Geology, v. 117, no. 104355, p. 1–14, https://doi.org/10.1016/j.marpetgeo.2020.104355.
Wedepohl, K.H., 1970, Geochemische Daten von sedimentaren Karbonaten und Karbonatgesteinen in ihrem faziellen und petrogenetischen Aussagewert: Verhandlungen Der Geologischen Bundesanstalt, v. 4, p. 692–705.
Wedepohl, K.H., 1971, Environmental influences on the chemical composition of shales and clays, *in* Ahrens, L.H., Press, F., Runcorn, S.K., and Urey, H.C., eds., Physics and Chemistry of the Earth: Oxford, UK, Pergamon Press Ltd, p. 307–331.
Wicander, E.R., 1974, Upper Devonian-lower Mississippian acritarchs and prasinophycean algae from Ohio, U.S.A: Palaeontographica B Palaeophytology, v. 148, p. 9–43.
Winchester, J.A., and Floyd, P.A., 1977, Geochemical discrimination of different magma series and their differentiation products using immobile elements: Chemical Geology, v. 20, p. 325–343, https://doi.org/10.1016/0009-2541(77)90057-2.
Winslow, M.R., 1962. Plant spores and other microfossils from Upper Devonian and Lower Mississippian rocks of Ohio. United States Geological Survey Professional Paper, 364, 1–93, https://doi.org/10.3133/pp364.

Wood, G.D., Gabriel, A.M., and Lawson, J.C., 1996, Palynological techniques: Processing and microscopy, *in* Jansonius, J., and McGregor, D.C., eds., Palynology: Principles and Applications: College Station, Texas, USA, American Association of Stratigraphic Palynologists Foundation, v. 1, p. 29–50.

Wyżga, B., 1987, Lower Palaeozoic of the Bardo Mountains (Sudetes): A sequence of deep- sea pelagic sediments: Geologica Sudetica, v. 22, p. 119–145.

Yang, S., Hu, W., and Wang, X., 2021, Mechanism and implications of upwelling from the Late Ordovician to early Silurian in the Yangtze region, South China: Chemical Geology, v. 565, no. 120074, p. 1–13, https://doi.org/10.1016/j.chemgeo.2021.120074.

Yudovich, Y.E., and Ketris, M.P., 2015, Geokhimicheskiye i Mineralogicheskiye Indikatory Vulkanogennykh Produktov v Osadochnykh Tolshchakh, second edition: Moscow, Russia, Direct Media, 724 p.

Zhang, L., Chen, D., Kuang, G., Guo, Z., Zhang, G., and Wang, X., 2020, Persistent oxic deep ocean conditions and frequent volcanic activities during the Frasnian-Famennian transition recorded in South China: Global and Planetary Change, v. 195, no. 103350, https://doi.org/10.1016/j.gloplacha.2020.103350.

Ziegler, W., 1962, Taxionomie und Phylogenie Oberdevonischer Conodonten und ihre stratigraphische Bedeutung: Abhandlunghen des Hessisches Landesamt für Bodenforschung, v. 38, p. 1–166.

Ziegler, W., and Huddle, J.W., 1969, Die *Palmatolepis glabra*—Groupe (Conodonta) nach der Revision der Typen von Ulrich & Bassler durch J.W. Huddle: Fortschritte in der Geologie von Rheinland und Westfalen, v. 16, p. 377–386.

Ziegler, W., and Sandberg, C.A., 1990, The Late Devonian standard conodont zonation: Courier Forschungsinstitut Senckenberg, v. 121, p. 1–115.

Zong, R., Wang, Z., Jiang, T., and Gong, Y., 2016, Late Devonian radiolarian-bearing siliceous rocks from the Karamay ophiolitic mélange in western Junggar: Implications for the evolution of the Paleo-Asian Ocean: Palaeogeography, Palaeoclimatology, Palaeoecology, v. 448, p. 266–278, https://doi.org/10.1016/j.palaeo.2015.10.006.

Science Editor: Rob Strachan
Associate Editor: Bradley Cramer

Manuscript Received 14 November 2020
Revised Manuscript Received 2 July 2021
Manuscript Accepted 28 October 2021

Printed in the USA